

Diplomarbeit

# Zungenmaus - Drahtlose Übertragung der Sensordaten

Hamza Ben Hassen

Geboren am: 9. Juli 1993 in Duisburg  
Matrikelnummer: 4114500  
Immatrikulationsjahr: 2014

zur Erlangung des akademischen Grades

**Diplomingenieur (Dipl.-Ing.)**

Betreuer

**Dipl.-Ing. Kathleen Große**

Betreuer Hochschullehrer

**Prof. Dr.-Ing. Peter Birkholz**

Eingereicht am: 5. November 2020

## **Aufgabenstellung für die Anfertigung einer Diplomarbeit**

Studiengang: Elektrotechnik  
Studienrichtung: AMR  
Name: **Hamza Ben Hassen**  
Matrikelnummer: 4114500  
Immatrikulationsjahr: 2014  
Titel: **Zungenmaus - Drahtlose Übertragung der Sensordaten**

### **Ziele der Arbeit**

Für die Entwicklung eines altersgerechten Assistenzsystems in Form einer Eingabe- und Steuerhilfe, welches die Hände zur Bedienung von Geräten überflüssig macht und diese durch die Zunge ersetzt (Zungenmaus), ist eine kabellose Übertragung von Sensordaten wünschenswert. Im Rahmen dieser Arbeit soll daher die prinzipielle Möglichkeit der drahtlosen Datenübertragung aus der Mundhöhle heraus untersucht werden.

### **Schwerpunkte der Arbeit**

- Ausführliche Literaturrecherche zum Stand der Forschung, dabei sollen folgende Punkte Beachtung finden:
  - Auswirkung von organischem Gewebe auf drahtlose Datenübertragung
  - Methoden zur Bewertung einer Funkstrecke
- Recherche für den geplanten Einsatz geeigneter **drahtloser** Sender und Empfänger, Darstellung der Unterschiede
- Auswahl eines geeigneten Transceivers für die Experimente
- Entwurf, Aufbau und Durchführung einer Messreihe zur Bestimmung der Sende- und Empfangscharakteristik in und aus der Mundhöhle in Abhängigkeit der geometrischen Anordnung und der elektrischen Leistungsaufnahme
- Aussagekräftige Darstellung und Diskussion der experimentellen Ergebnisse

Die Arbeit wird in deutscher Sprache verfasst.

Erstgutachter: Prof. Dr.-Ing. Peter Birkholz  
Zweitgutachter: Prof. Dr.-Ing. habil. Ercan Altinsoy  
Betreuer: Dipl.-Ing. Kathleen Große  
Ausgehändigt am: 1. Juni 2020  
Einzureichen am: 5. November 2020

Prof. Dr.-Ing. Peter Birkholz  
Betreuer Hochschullehrer

## Selbständigkeitserklärung

Ich erkläre hiermit ehrenwörtlich, dass ich die vorliegende Arbeit selbstständig angefertigt habe. Die aus fremden Quellen direkt oder indirekt übernommenen Gedanken sind als solche kenntlich gemacht. Es wurden keine anderen als die angegebenen Quellen und Hinweise verwendet.

Die vorliegende Arbeit wurde bisher keiner anderen Prüfungsbehörde vorgelegt und auch noch nicht veröffentlicht.

Dresden, der 19th November 2020

Hamza Ben Hassen

## Abstract

This work presents a feasibility analysis for implementing a wireless data link from inside the mouth cavity using off the shelf components. Such a wireless link is purposed to enable new wireless assistive devices operated by the tongue for people suffering from reduced dexterity due to illness or accidents. An evaluation prototype is built using off the shelf components and is evaluated by measuring the transmitted signal intensity and the wireless data rate in an vivo environment.

## Abstrakt

In dieser Arbeit wird eine Machbarkeitsanalyse für die Implementierung einer drahtlosen Datenverbindung aus dem Inneren der Mundhöhle unter Verwendung von Standardkomponenten vorgestellt. Eine solche drahtlose Verbindung soll neue drahtlose, mit der Zunge bedienbare Hilfsgeräte für Menschen ermöglichen, die aufgrund von Krankheiten oder Unfällen unter eingeschränkter Handfertigkeit leiden. Ein Evaluierungsprototyp wird unter Verwendung von Standardkomponenten gebaut und durch Messung der übertragenen Signalintensität und der drahtlosen Datenrate in einer In-vivo-Umgebung evaluiert.

—

# Contents

<b>1</b>	<b>Introduction</b>	<b>1</b>
1.1	Motivation . . . . .	1
1.2	Objectives and goals . . . . .	2
<b>2</b>	<b>Literature Survey</b>	<b>3</b>
2.1	History of wireless information transfer . . . . .	3
2.2	State of the art . . . . .	6
2.2.1	Small wireless devices . . . . .	7
2.2.2	Intra-oral implementations . . . . .	7
<b>3</b>	<b>Theory</b>	<b>9</b>
3.1	Electromagnetic waves . . . . .	9
3.2	Dielectric properties of matter . . . . .	12
3.2.1	Complex dielectric constant . . . . .	13
3.2.2	Dielectric relaxation . . . . .	17
3.3	Intra-oral environment . . . . .	18
3.4	Reflection at the interfaces . . . . .	19
3.4.1	Transmission line model . . . . .	21
3.5	Quality metrics for wireless links . . . . .	24
<b>4</b>	<b>Methods</b>	<b>26</b>
4.1	Design Considerations . . . . .	26
4.1.1	Antenna . . . . .	26
4.1.2	Power . . . . .	27
4.2	Implementation . . . . .	28
4.2.1	Transmitter . . . . .	29
4.2.2	Receiver . . . . .	31
4.2.3	Data acquisition and visualisation . . . . .	33
<b>5</b>	<b>Measurements</b>	<b>37</b>
5.1	Radiation pattern . . . . .	37
5.2	Throughput measurement . . . . .	37
5.3	Signal strength measurement . . . . .	37
5.4	Packets per Second . . . . .	37

5.5 Validation . . . . .	37
5.6 Antenna Performance . . . . .	38
<b>6 Evaluation</b>	<b>41</b>
6.1 Antenna performance . . . . .	41
6.1.1 Reflection coefficient . . . . .	43
6.2 Radio system performance . . . . .	44
6.2.1 Radiation pattern . . . . .	44
6.2.2 Data rate . . . . .	46
6.2.3 Power consumption . . . . .	47
<b>7 Discussion</b>	<b>49</b>
7.1 Potential improvements . . . . .	50
7.2 Overview and potential application . . . . .	50
<b>Glossar</b>	<b>52</b>
<b>Bibliography</b>	<b>52</b>

# List of Figures

2.1	Modulated back scattering principle . . . . .	4
2.2	Semaphore in 18th-century France. . . . .	4
2.3	Modulated back-scattering principle . . . . .	5
2.4	Heinrich Hertz's Apparatus for detecting electromagnetic waves . . . . .	6
2.5	iTDS overview . . . . .	8
3.1	Propagation mechanism . . . . .	10
3.2	Forward propagating wave . . . . .	10
3.3	Penetration depth versus frequency for some tissues . . . . .	13
3.4	Dispersion of biological tissues . . . . .	17
3.5	Frontal view of the mouth . . . . .	18
3.6	Muscular structures of the face . . . . .	19
3.7	radio system circuit . . . . .	20
3.8	Oral mucosa structure . . . . .	20
3.9	complex dielectric permittivity of saliva . . . . .	21
3.10	radio system circuit . . . . .	21
3.11	Two-wire transmission line . . . . .	22
3.12	Two-port network . . . . .	24
3.13	Typical wireless structure . . . . .	24
4.1	Transmitter components . . . . .	28
4.2	Antenna Evaluation . . . . .	30
4.3	Transmitter components . . . . .	31
4.4	Receiver Control Interface . . . . .	32
4.5	. . . . .	34
5.1	Throughput measurement routine . . . . .	38
5.2	Antenna Evaluation . . . . .	39
5.3	Antenna characterization environment . . . . .	39
5.4	Radiation Pattern . . . . .	40
6.1	Measured S11 . . . . .	42
6.2	Radiation Pattern . . . . .	43
6.3	Radiation Pattern Horizontal . . . . .	44

6.4	Radiation Pattern Vertical . . . . .	44
6.5	Measured RSSI . . . . .	45
6.6	Radiation pattern - RSSI . . . . .	46
6.7	Throughput measurement . . . . .	47

# List of Tables

3.1	Dielectric properties of tissues . . . . .	19
4.1	Overview small batteries . . . . .	27
4.2	Common sensors power consumption . . . . .	28
4.3	Overview BLE SiP solutions . . . . .	29
4.6	Wireless Quality Tool Used Libraries . . . . .	33
4.4	Overview BLE SoC solutions . . . . .	35
4.5	Command Line Interface Commands . . . . .	36
6.1	Antenna evaluation configurations . . . . .	41
6.2	Wireless Quality Tool Used Libraries . . . . .	47

# Nomenclature

BLE Bluetooth Low Energy

CLI Command Line Interface

LoRa Long Range Radio

PPS Packets Per Second

RSSI Received Signal Strength Indication

SiP system-in-package

SNR Signal to Noise Ratio

SoC System-on-a-Chip

# **1** Chapter 1

---

# **Introduction**

## **1.1 Motivation**

In the earlier days of computers, input modalities were very limited. At first software is programmed by manually wiring the computer and then an operation is executed, similar to a simple calculator. The invention of screen allowed a more dynamic interaction with computers in forms of command line interfaces operated with keyboards. The computer mouse was invented in 1964 and provided a new way of interacting with a computer, the graphical user interface. In a GUI, the mouse is operated to move a cursor on the screen. Mouse actions such as clicking or dragging an element trigger a command on the selected object. More recently touch screens are found on handheld computers and computer monitors. Instead of pointing to an element with the mouse cursor, the user directly touches the GUI element and triggers a command. The development of multitouch capable screens present in more recent devices more natural set of interactions is unlocked, such pinching to zoom or rotating an image.

All these modalities rely solely on hands, which makes them unavailable to people with reduced dexterity. Several factors can result in the inability to use the input modalities. Hand control might be deteriorated in the presence of extreme shaking. Additionally this way of interacting with a computer remains limited in terms of the achievable bandwidth. In recent years the advances in speech recognition and synthesis allowed a more natural way of interacting with computers. Good recognition accuracy could be achieved in modern handheld devices. However this method rely on producing vocal speech, which might not always be possible or wanted. This motivates the research of alternative input modalities. The ultimate input modality would be a brain computer interface. Even though a considerable effort have been put by researchers to implement such an interface, much more is still left to be done. Alternatively silent speech can be considered. In silent speech the non vocal articulations of speech, such as moving the tongue, the lower jaw or the lips are used to reconstruct the intended words. This can be used in the context of alternative input modalities.

The tongue is a flexible muscle that is usually robust against illness. In a previous work the principle of using the tongue to produce repeatable patterns to be used as computer commands is evaluated. It was concluded that it was relatively easy to use tongue gestures to operate an optimized user interface.

In this work the possibility of wirelessly transmitting data from inside the mouth cavity is evaluated.

## 1.2 Objectives and goals

The present work explores the feasibility of implementing a robust and low-powered wireless link from inside the mouth cavity. The purpose of the this thesis is thus to gain a deeper knowledge of the topic and to create an evaluation prototype using off the shelf components. For this the following objectives are defined :

- Review state of the art implementations of intra-oral wireless devices.
- Review the basics of electromagnetic radiation and its usage for wireless information transfer.
- Review models of electric properties of human body tissues in radio frequencies, with a focus on tissues in the mouth cavity.
- Quantify the losses introduced by placing an antenna inside the mouth.
- Survey wireless quality criterion.
- Select a transmitter and a receiver to conduct a series of measurements.

# **2** Chapter 2 **Literature Survey**

---

## **2.1 History of wireless information transfer**

Collaboration between living species requires a wireless transmission of information. Observing nature we can identify several forms of such communications. First we identify acoustic methods. Information is encoded in the alteration of air pressure caused by sound from acoustic organs or mechanical actions. This perturbation is transported as an acoustic wave at the speed of sound to an ear that transforms it into an electric signal that reaches the brain, and a sound is experienced. Several animals use this principle to communicate the presence of predators or food. Human invented languages to convey a broader set of concepts and ideas using this method.

A different approach is observed in nature. Electromagnetic radiation reflecting off the surface of objects is altered. The geometric and physical properties of matter result in a frequency selective absorption of radiation. An eye detects these alterations and colours and shapes are experienced. Through the controlled manipulation of the geometric and electric properties of a reflecting object, called a transponder, information can be coded and transmitted wirelessly, at the speed of light. Such forms of wireless communication are referred to as back scattering techniques. Figure 2.1 illustrates this principle.

Back in 1792, Claude Chappe invented the semaphore telegraph in France that used this principle. The working principle of the semaphore is based on several towers spread between cities. In each tower human operators spell words through the manipulation of the semaphore arms. The message is reproduced at the next tower to relay the message. Figure 2.2 illustrates the working principle of the semaphore.

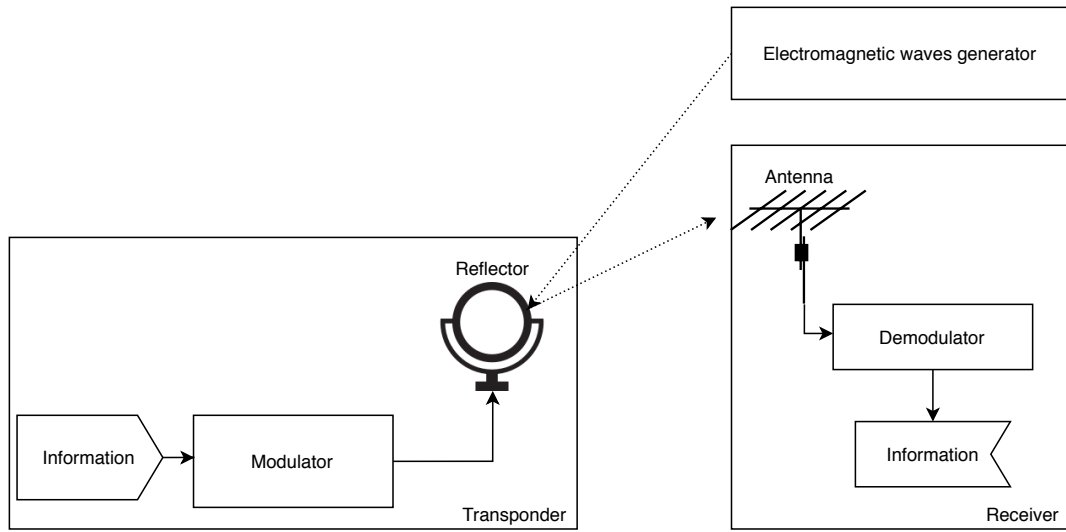


Figure 2.1: Modulated back-scattering principle. This technique works by reflecting an electromagnetic wave on a transponder. The transponder reflects the incident wave and adds a controlled distortion to the signal. The receiver intercepts the reflected signal and detects the information coded into the distortion.

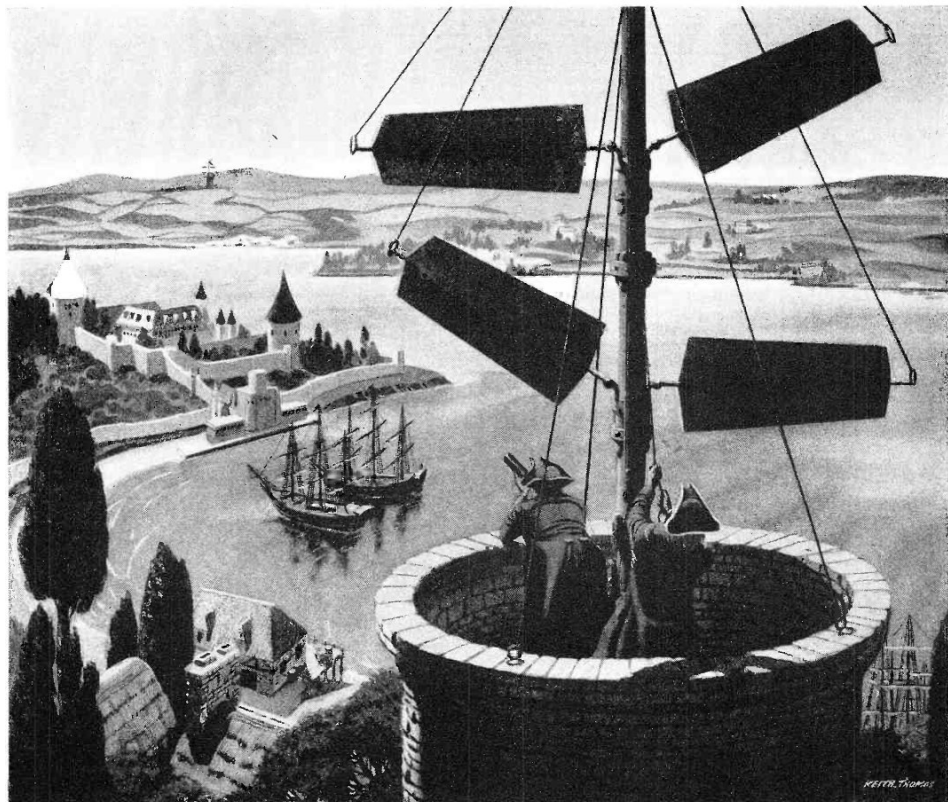


Figure 2.2: Semaphore in 18th-century France. The operators would move the semaphore arms to successive positions to spell out text messages in semaphore code. In the next tower the semaphore arms are observed through binoculars to decode the sent message. The drawing is signed "Keith Thomas" in lower right corner - Image retrieved from <http://www.americanradiohistory.com>

Vision can be considered as a wireless communication system following this principle. The universe communicates shapes and colors through the reflection of electromagnetic radiation off objects onto an eye.

Another device using this principle is the Photophone invented in 1880 by Alexander Graham Bell. This device is a wireless audio communication system that works by modulating the sun light with speech information. At the receiver the information can be decoded and the original speech reconstructed. Figure 2.3 illustrates the working principle of the Photophone. The first transmitted phrase was transmitted wirelessly over a distance of 213 meters by bell's assistant Sumner Tainter and stated: " Mr. Bell, if you hear what I say, come to the window and wave your hat." [1].

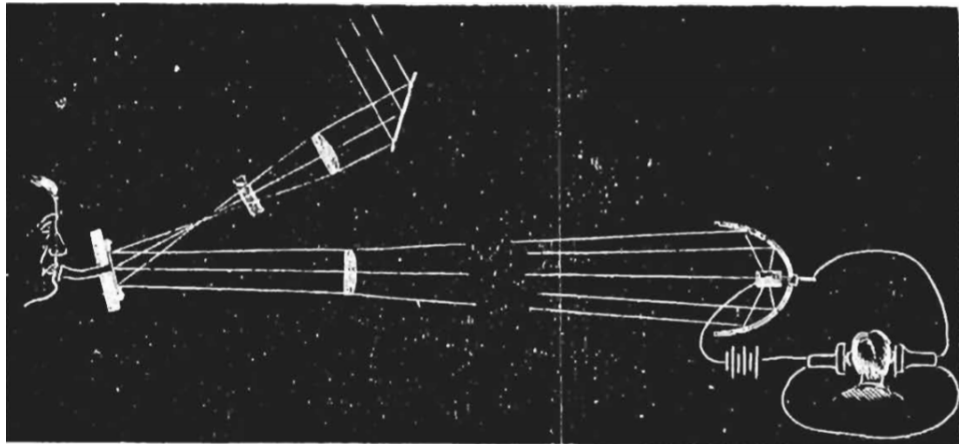


Figure 2.3: Alexander Graham Bell's photophone in 1880. This device works by speaking in proximity to a flexible mirror. Acoustic waves resulting from speech vibrate the mirror and result in a varying reflected light intensity. The receiver transforms the varying light intensity to a time varying current driving an earphone to reproduce the original speech .[1]

Several milestones laid the foundation for modern wireless communication methods using electromagnetic waves. In 1785, Charles Augustin de Coulomb reported that the force between two point charges is directly proportional to the product of the magnitudes of the charges and inversely proportional to the square of the distance between them. Later in 1800 Alessandro Volta invented the first battery proving that electricity could be produced chemically. Volta's invention allowed further experimentation with direct electric current. In 1820 Hans Christian Ørsted published his discovery that a compass needle moves in the presence of a current carrying wire. This confirmed the direct relationship between electricity and magnetism. Furthering Ørsted's experimental work, André-Marie Ampère showed that two parallel wires conducting current attract or repel each other depending on the direction of the current. He formulated these experimental results in what came to be known as Ampère's law, which states that the magnetic field around an electric current is proportional to the electric current intensity. In 1831 Michael Faraday showed that drawing a magnet through a loop of a conducting wire

induces current in the wire. He established that “line of forces” surrounded the magnet and were responsible for the electromagnetic phenomena. Faraday also hypothesized that light was an electromagnetic phenomena.

James Clerk Maxwell incorporated all prior results in his electromagnetic theory that united electricity and magnetism in 1864. Maxwell’s original formulation of electromagnetism contained 20 equations. Heaviside later reformulated Maxwell’s equation in their present form. In 1879 Hermann von Helmholtz published a prize problem in the Prussian Academy of Science in Berlin to motivate an experimental validation of Maxwell’s theory. Heinrich Rudolf Hertz reflected on the problem but gave up initially, thinking it was too difficult. In 1887 Hertz was able to solve the problem by proving RF currents in dielectric materials [2]. Later in 1888 Hertz carried out his experiment to prove the existence of these waves first success work laid the foundation for our modern wireless technologies. Initially Maxwell’s work went unnoticed for several years, mainly due to the complexity of his formulation. In 1888 Hertz was able to verify the existence of electromagnetic waves in air using a spark gap oscillator. The spark gap oscillator consists of a metal rod with a small gap in the midpoint. When sparks crossed these gaps high frequency oscillation were transmitted through the air. He detected these oscillations using a similar structure at a distance. The apparatus used by Hertz is illustrated in figure 2.4

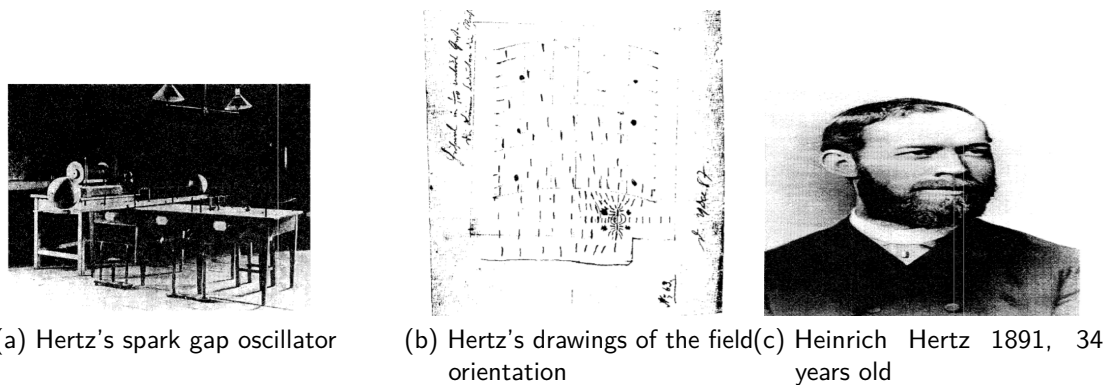


Figure 2.4

Hertz did not realize the usefulness of his discovery. In fact he commented “ I do not think that the wireless waves I have discovered will have any practical application.”[3]

## 2.2 State of the art

Today we live in an increasingly wireless environment with an abundance of wearable and IoT devices. Small wireless devices have been used in several contexts, such in implantable devices for health care applications or for tracking the behaviour of small

insects. In the first section we survey the smallest and lowest powered wireless devices. In the second section we focus on intra-oral implementations.

### **2.2.1 Small wireless devices**

In [4] a wireless transmitter based on Bluetooth low energy is presented. The transmitter is reported to consume 0.61 mW of power while transmitting at -8.4 dBm. The transmitter was implemented in a 4.5mmx18.6mm circuit board and demonstrated an advertising range of 8m.

### **2.2.2 Intra-oral implementations**

Wireless intra-oral devices have seen an interest in the literature. We identify implementations based on passive and active RFID [5] [6] [7] [8].

The earliest implementation of an intra-oral wireless device dates back to 2007 [9]. This implementation used the ZigBee protocol but the wireless link quality was not characterised. At the time Zigbee offered an advantage against Bluetooth 2.0 in terms of range and power consumption. Other implementations [10, 11, 12] use radio waves in the 2.4 GHz to relay data from a transmitter mounted under the hard palate. These implementations only prove the ability of using 2.4Ghz to penetrate the mouth cavity structures to nearby receivers ( $< 1 \text{ m}$ ), however no details about the signal attenuation, quality of wireless links or the achieved range were presented.

More recently in [13] a wireless intra oral device for monitoring sodium Intake is presented. This implementation uses Bluetooth Low Energy (BLE) for transmitting the measurements from a flexible PCB attached on a dental retainer and placed under the hard palate. In [14] Several RF frequencies in the ISM band were compared for intra oral usage. In [15] several antennas types were compared for the frequency Band ISM 2.4GHz.

The most advanced intraoral wireless device was presented in [16]. An overview of this implementation is illustrated in figure 2.5This implementation uses 3 frequency bands that are automatically switched to mitigate the effects of interference. A Custom Application-specific integrated circuit implements an adaptive impedance matching algorithim to mitigate the detuning effects during normal mouth movement. An operating range of 103 cm is reported with a transmit power consumtion of 11.52 mW.

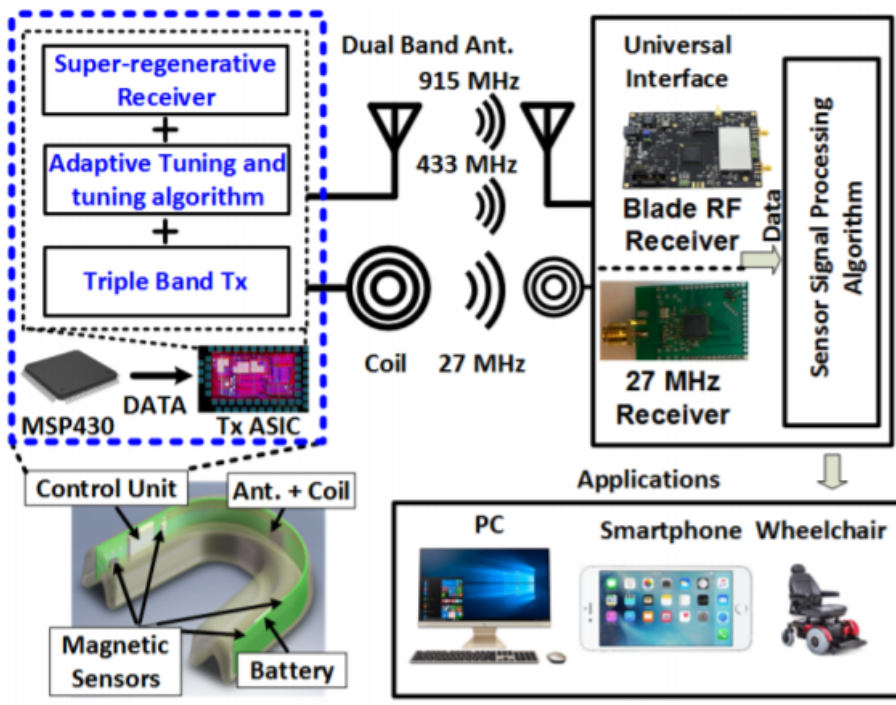


Figure 2.5: System overview of the intraoral Tongue Drive System [16]

# 3 Chapter 3

# Theory

This chapter introduces the models needed to understand the electromagnetic phenomena involved in the working of a radio transmitter. The goal of this chapter is to provide a discussion about the physical parameters involved in the propagation of an electromagnetic wave through a lossy medium , and the effects caused by placing an antenna close to body tissues.

The first part introduces the electromagnetic phenomena involved in the working of a radio transmitter. The interaction of electromagnetic waves with matter in general is discussed to introduce the loss factors.

The second part investigates the electric properties of biological tissues in general and provides a model for a layered structure simulating the area of interest in the mouth cavity.

The third part introduces necessary concepts and quantities from RF systems to understand the components of a wireless link and typically used performance criteria.

## 3.1 Electromagnetic waves

The concepts discussed in this section are based on [17, 18, 19]

At a fundamental level , an electromagnetic wave is the manifestation of the acceleration of charge. To transmit information wirelessly using electromagnetic waves, a charge quantity is modulated with information by controlling a current density  $\vec{J}$  in a conductive element, called an antenna.

A changing current density  $\vec{J}$  creates a changing magnetic field intensity  $\vec{H}$  according to bio-savart law, which through Faraday's law generates a time changing electric field intensity  $\vec{E}$ . This changing electric field now generates a changing magnetic field according to Ampéres law, and thus the wave propagates.

To study the interaction between the antenna and the biological tissues in the mouth cavity , the following approach is used. First the case of an electromagnetic wave propagating in lossy matter is modelled using the Maxwell's equations to obtain a metric qu The Maxwell's equations are used to introduce necessary quantities. In the

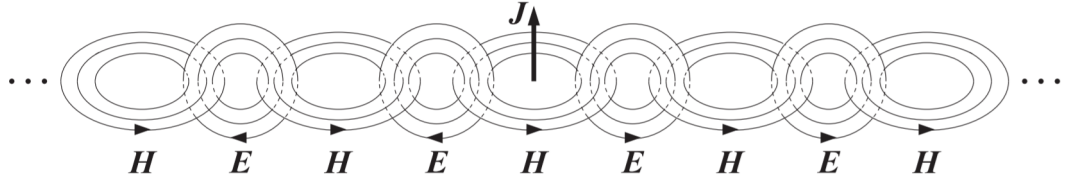


Figure 3.1: Propagation mechanism of an electromagnetic waves generated by an current current distribution  $\vec{J}$  [17]

next part an electromagnetic wave propagating in a lossy medium is discussed. Finally the effects of proximity of the antenna to biological tissues are discussed.

The Maxwell's equations formulate this behaviour. We first consider

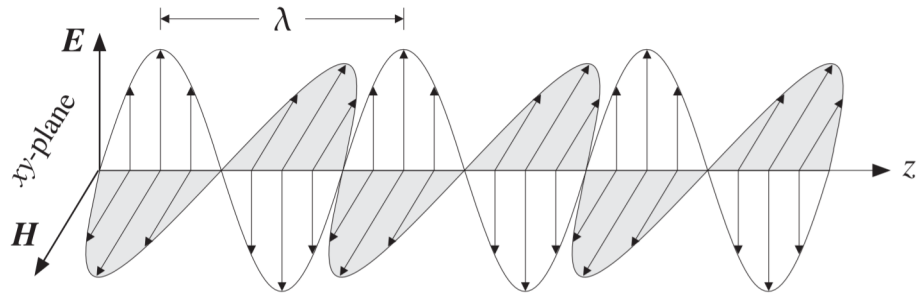


Figure 3.2: Forward uniform plane wave. [17]

The frequency domain formulation is used.

$$\vec{\nabla} \cdot \vec{D} = \rho \quad (3.1)$$

$$\vec{\nabla} \cdot \vec{B} = 0 \quad (3.2)$$

$$\vec{\nabla} \times \vec{E} = -j\omega \vec{B} \quad (3.3)$$

$$\vec{\nabla} \times \vec{H} = \vec{J} + j\omega \vec{D} \quad (3.4)$$

The quantities  $\vec{E}$  and  $\vec{H}$  are the electric and magnetic field intensities and have the units of  $[\frac{\text{volt}}{\text{meter}}]$  and  $[\frac{\text{ampere}}{\text{meter}}]$  respectively. The quantities  $\vec{D}$  and  $\vec{B}$  are the electric and magnetic flux densities and have the units of  $[\frac{\text{coulomb}}{\text{meter}^2}]$  and  $[\frac{\text{weber}}{\text{meter}^2}]$ <sup>1</sup> respectively.

The quantity  $\vec{J}$  measured  $[\frac{\text{ampere}}{\text{meter}^2}]$  denotes the conduction current density and is related to the electric field  $\vec{E}$  as  $\vec{J} = \sigma \vec{E}$  where  $\sigma$  is defined as the conductivity. The conductivity

<sup>1</sup> $[\frac{\text{weber}}{\text{meter}^2}]$  is equivalent to  $[\text{tesla}]$

is a property of the medium of propagation. In vacuum and non conducting media  $\sigma = 0$ . The quantity  $\rho$  and  $\vec{J}$  are the total electric charge density and total electric current density of the medium in  $[\frac{\text{coulomb}}{\text{meter}^3}]$  and  $[\frac{\text{ampere}}{\text{meter}^2}]$  respectively. In free space the constitutive relations relating  $\vec{D}$  and  $\vec{B}$  to  $\vec{E}$  and  $\vec{H}$  are :

$$\vec{D} = \varepsilon_0 \vec{E} \quad (3.5)$$

$$\vec{H} = \frac{\vec{B}}{\mu_0} \quad (3.6)$$

with  $\varepsilon_0$  the electric permittivity  $\mu_0$  the magnetic permeability in vacuum.

$$\varepsilon_0 = 8.854 \times 10^{-12} \text{ farad/m}$$

$$\mu_0 = 4\pi \times 10^{-7} \text{ henry/m}$$

we can further define speed of light and characteristic impedance of vacuum:

$$c_0 = \frac{1}{\sqrt{\varepsilon_0 \mu_0}} = 3 \times 10^8 \frac{\text{m}}{\text{s}}$$

$$\eta_0 = \sqrt{\frac{\mu_0}{\varepsilon_0}} = 377 \text{ ohm}$$

When the wave propagates in matter the constitutive relations relating  $\vec{D}$  and  $\vec{B}$  to  $\vec{E}$  and  $\vec{H}$  are dependent on material properties.

## Propagation in a lossy medium

A wave propagating in a lossy medium results in a conduction current  $\vec{J}_{cond} = \sigma \vec{E}$  and a displacement current  $\vec{J}_{disp} = j\omega \vec{D}$ .

Isotropic and linear materials are considered to define the constitutive equations in matter. This is a realistic approximation of biological tissues in high frequencies [20].

with  $\varepsilon$  the electric permittivity in  $[\frac{\text{farad}}{\text{meter}}]$ ,  $\sigma$  the conductivity in  $[\frac{\text{siemens}}{\text{meter}}]$  and  $\mu$  the magnetic permeability in  $[\frac{\text{henries}}{\text{meter}}]$ .

Applying the curl operator to 3.3 and using 3.6 :

$$\vec{\nabla} \times \vec{\nabla} \times \vec{E} = \vec{\nabla}(\vec{\nabla} \cdot \vec{E}) - \nabla^2 \vec{E} = -j\omega \mu \vec{\nabla} \times \vec{B} \quad (3.7)$$

using 3.4 and 3.1 and 3.5 yields :

$$\nabla^2 \vec{E} - j\omega\mu(\sigma + j\omega\varepsilon)\vec{E} = \vec{\nabla}(\rho/\varepsilon) \quad (3.8)$$

The quantity  $j\omega\mu(\sigma + j\omega\varepsilon)$  is defined as  $\gamma^2$ , where :

$$\gamma = \sqrt{j\omega\mu(\sigma + j\omega\varepsilon)} = \alpha + j\beta \quad (3.9)$$

is the propagation constant.

$\alpha$  and  $\beta$  are defined as the attenuation constant and the phase constant.

Solving 3.9 for  $\alpha$  and  $\beta$  yields :

$$\alpha = \omega\sqrt{\mu\varepsilon} \left[ \frac{1}{2} \left( \sqrt{1 + \frac{\sigma^2}{\varepsilon^2\omega^2}} - 1 \right) \right]^{\frac{1}{2}} \quad (3.10)$$

$$\beta = \omega\sqrt{\mu\varepsilon} \left[ \frac{1}{2} \left( \sqrt{1 + \frac{\sigma^2}{\varepsilon^2\omega^2}} + 1 \right) \right]^{\frac{1}{2}} \quad (3.11)$$

Equation 3.10 can be used to introduce the skin depth defined as :

$$\delta = \frac{1}{\alpha}$$

The skin depth of a material  $\delta$  describes the depth at which amplitude of a penetrating wave has decayed by a factor of  $1/e$  of its initial value. In figure 3.3 the penetration depth of some biological tissues is illustrated:

## 3.2 Dielectric properties of matter

When a constant electric field is applied to a system of charges, such as in a biological tissue, the charges are displaced in a manner dependent on whether the charges are free or bound. Free charges lead to the translation of positive charges in the direction of the applied field, and negative charges in the opposite direction. Bound charges are pairs of positive and negative charges called dipoles are rotated in the presence of the applied field. This rotation induces a displacement current that is transient and only lasts until the dipoles are aligned with the applied field and reach an equilibrium. The polarisation of charges takes times to develop and thus can be described as a relaxation process.

In the first part we consider a simple model of the displacement of charges to introduce the complex dielectric constant. Then we introduce the relaxation process responsible

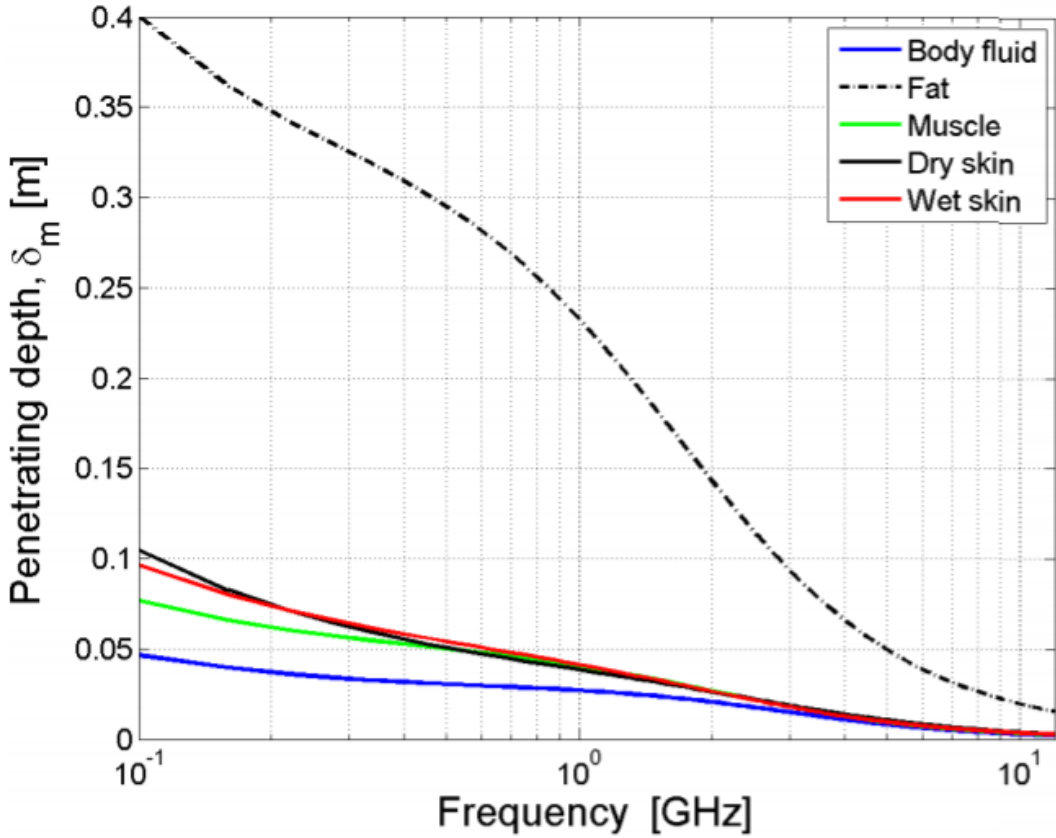


Figure 3.3: Penetration depth versus frequency for some tissues[21]

for the dispersive properties this complex dielectric properties. Finally we consider the dielectric properties of tissues present in the intra-oral environment to gain insights about optimal antenna placement.

### 3.2.1 Complex dielectric constant

The dynamics of this movement of charges give rise the dielectric properties of the material and characterise its behavior in the presence of an electric field. To introduce these concepts mathematically, we consider a simple model of the displacement of an electron bound to its nucleus, as provided in [17].

$$\ddot{x} + \gamma\dot{x} + \omega_0^2x = \frac{e}{m}E(t) \quad (3.12)$$

$E(t)$  represents the applied electric field and is assumed to only have an  $x$  component and a sinusoidal time dependency with frequency  $\omega$  so that  $E(t) = E_0e^{j\omega t}$ .

The binding between the electron and the nucleus is modeled as a spring force through the term  $\omega_0^2x$ , with  $\omega_0$  the resonance frequency of the spring defined by  $\omega_0 = \sqrt{\frac{k}{m}}$ . A

friction term  $\gamma \dot{x}$  represents the collisions that tend to slow down the electron. The parameter  $\gamma$  is a measure of the rate of collisions per unit time.

Replacing time derivatives  $\partial t$  by  $j\omega$ , we obtain the following expression of 3.12:

$$-\omega^2 x + j\omega\gamma x + \omega_0^2 x = \frac{e}{m} E \quad (3.13)$$

Solving 3.13 for  $x$  yields:

$$x = \frac{\frac{e}{m} E}{-\omega^2 + j\omega\gamma + \omega_0^2} \quad (3.14)$$

From equation 3.14 a polarization per unit volume  $P$  can be introduced. Under the assumption that there are  $N$  elementary dipoles per unit volume, with the electric dipole moment  $p = ex$ ,  $P$  can be written as :

$$P = Np = Nex = \frac{N \frac{e^2}{m} E}{-\omega^2 + j\omega\gamma + \omega_0^2} \equiv \varepsilon_0 \chi(\omega) E \quad (3.15)$$

The electric flux density is then:

$D = \varepsilon_0 E + P \equiv \varepsilon(\omega) E$  where  $\varepsilon(\omega)$  the effective permittivity defined as :

$$\varepsilon(\omega) = \varepsilon_0 + \frac{\varepsilon_0 \omega_p^2}{-\omega^2 + j\omega\gamma + \omega_0^2} \quad (3.16)$$

The term  $\omega_p$  denotes the plasma frequency of the material , defined as :

$$\omega_p^2 = \frac{Ne^2}{\varepsilon_0 m}$$

The electric susceptibility  $\chi(\omega)$  defined through  $\varepsilon(\omega) = \varepsilon_0(1 + \chi(\omega))$  can be written as:

$$\chi(\omega) = \frac{\omega_p^2}{-\omega^2 + j\omega\gamma + \omega_0^2} \quad (3.17)$$

Taking the limit  $\omega \rightarrow 0$  in 3.16 we obtain the nominal dielectric constant :

$$\varepsilon(0) = \varepsilon_0 + \frac{Ne^2}{m\omega_0^2} \quad (3.18)$$

From 3.16 we can notice that  $\varepsilon(\omega)$  is complex valued, and can be written as :

$$\varepsilon(\omega) = \varepsilon'(\omega) - j\varepsilon''(\omega) \quad (3.19)$$

$\varepsilon'(\omega)$  and  $\varepsilon''(\omega)$  denote the refractive and absorptive properties of the material. It follows from 3.16:

$$\varepsilon'(\omega) = \varepsilon_0 + \frac{\varepsilon_0 \omega_p^2 (\omega_0^2 - \omega^2)}{(\omega^2 - \omega_0^2)^2 + \gamma^2 \omega^2} \quad (3.20a)$$

$$\varepsilon''(\omega) = \varepsilon_0 + \frac{\varepsilon_0 \omega_p^2 \gamma \omega}{(\omega^2 - \omega_0^2)^2 + \gamma^2 \omega^2} \quad (3.20b)$$

From equation 3.14 we can extract the electron velocity:

$$v = j\omega x = \frac{j\omega \frac{e}{m} E}{-\omega^2 + j\omega\gamma + \omega_0^2} \quad (3.21)$$

Using the relationship  $\vec{J} = \rho v$ , with  $\rho$  the volume density defined by  $\rho = Ne$ , and the relationship  $\vec{J}_{cond} = \sigma(\omega) \vec{E}$ , we can write the conductivity current density as:

$$J_{cond} = \rho v = N e v = \frac{j\omega N \frac{e^2}{m} E}{-\omega^2 + j\omega\gamma + \omega_0^2} \equiv \sigma(\omega) \vec{E} \quad (3.22)$$

The conductivity  $\sigma(\omega)$  can then be written as :

$$\sigma(\omega) = \frac{j\omega N \frac{e^2}{m}}{-\omega^2 + j\omega\gamma + \omega_0^2} = \frac{j\omega \varepsilon_0 \omega_p^2}{-\omega^2 + j\omega\gamma + \omega_0^2} \quad (3.23)$$

Since the conduction current result from the unbound electrons, the binding force modeled by the term  $\omega_0$  is ignored. The conductivity is then defined by :

$$\sigma(\omega) = \frac{\varepsilon_0 \omega_p^2}{\gamma + j\omega} \quad (3.24)$$

The model defined by 3.24 is known as the “Drude model”.

Similarly to 3.18, we can define a nominal conductivity for  $\omega \rightarrow 0$  :

$$\sigma(0) = \frac{\varepsilon_0 \omega_p^2}{\gamma} = \frac{Ne^2}{m\gamma}$$

The term  $\sigma(\omega)/j\omega$  is the electric susceptibility defined in 3.17. A relationship between the conductivity  $\sigma(\omega)$  and the permittivity  $\varepsilon(\omega)$  can then be obtained:

$$\varepsilon(\omega) = \varepsilon_0 + \frac{\varepsilon_0 \omega_p^2}{-\omega^2 + j\omega\gamma + \omega_0^2} = \varepsilon_0 - \frac{j\sigma(\omega)}{\omega} \quad (3.25)$$

Materials with both dielectric and conductive properties can be described by both the polarization of bound charges and the conduction of unbound charges. This can be

modeled by introducing the total effective permittivity by combining 3.16 and 3.24 and assuming different parameters prefixed by d and c for displacement and conduction:

$$\varepsilon(\omega) = \varepsilon_0 + \frac{\varepsilon_0 \omega_{dp}^2}{-\omega^2 + j\omega\gamma_d + \omega_{d0}^2} + \frac{\varepsilon_0 \omega_{cp}^2}{j\omega(\gamma_c + j\omega)} \quad (3.26)$$

Equation 3.26 can be more conveniently written as:

$$\varepsilon(\omega) = \varepsilon_d(\omega) + \frac{\sigma_c(\omega)}{j\omega} \quad (3.27)$$

with  $\varepsilon_d(\omega) = \varepsilon_0 + \frac{\varepsilon_0 \omega_{dp}^2}{-\omega^2 + j\omega\gamma_d + \omega_{d0}^2}$  and  $\sigma_c(\omega) = \frac{\varepsilon_0 \omega_{cp}^2}{(\gamma_c + j\omega)}$

From 3.20a  $\varepsilon_d(\omega) = \varepsilon'_d(\omega) - j\varepsilon''_d(\omega)$  we obtain

$$\varepsilon(\omega) = \varepsilon'_d(\omega) - j\varepsilon''_d(\omega) + \frac{\sigma_c(\omega)}{j\omega} \quad (3.28)$$

The complex permittivity is more typically denoted in the complex form:

$$\varepsilon(\omega) = \varepsilon'(\omega) - j\varepsilon''(\omega) \quad (3.29)$$

assuming real valued conductivity  $\sigma_c(\omega)$  in the frequency range of interest, we obtain from 3.28:

$$\varepsilon'(\omega) = \varepsilon'_d(\omega) = \varepsilon_r \quad (3.30a)$$

$$\varepsilon''(\omega) = \varepsilon''_d(\omega) + \frac{\sigma_c(\omega)}{\omega} = \frac{\sigma}{\omega\varepsilon_0} \quad (3.30b)$$

The imaginary part  $\varepsilon''$  of the complex permittivity is known as the loss factor. The real part  $\varepsilon'(\omega)$  is typically denoted as the relative dielectric constant.

The total current density can be written as :

$$J_{tot} = j\omega\varepsilon(\omega)E \quad (3.31)$$

The attenuation of an electromagnetic wave propagating in matter is due to the total current density of the displacement and the conduction currents. The ohmic losses resulting from these currents can be written as:

$$\frac{dP_{loss}}{dV} = \frac{1}{2}\Re[J_{tot}E^*] = \frac{1}{2}\omega\varepsilon''(\omega)|E|^2 \quad (3.32)$$

The loss tangent is typically used to quantify the ohmic losses and is defined as :

$$\tan\theta = \frac{\varepsilon''(\omega)}{\varepsilon'(\omega)} \quad (3.33)$$

using 3.30a and 3.30b the loss tangent can be represented as the sum of the loss tangents resulting from conduction and displacement:

$$\tan\theta = \frac{\varepsilon''(\omega)}{\varepsilon'(\omega)} = \frac{\sigma_c(\omega)}{\omega\varepsilon'_d(\omega)} + \frac{\varepsilon''_d(\omega)}{\varepsilon'_d(\omega)} = \tan\theta_c + \tan\theta_d \quad (3.34)$$

A large loss tangent means the material is highly lossy.

### 3.2.2 Dielectric relaxation

As seen from the previous section, the dielectric properties of matter show a dependency on frequency. This property is called dispersion. Biological tissues exhibit several dispersions as illustrated in figure 3.4.

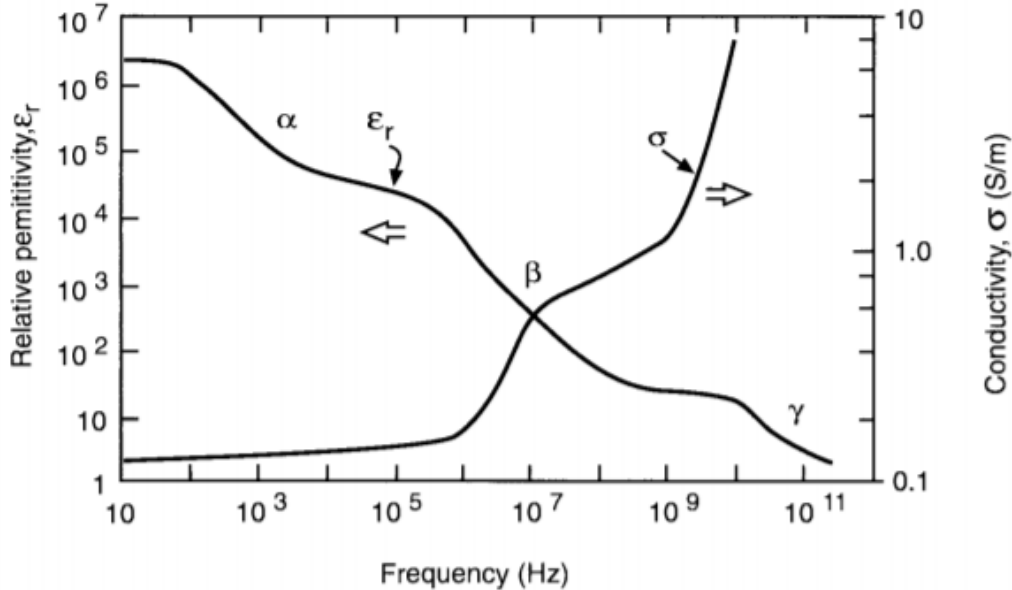


Figure 3.4: Frequency variation of complex permittivity in biological tissues[22]

Of interest in this thesis is the  $\gamma$  dispersion that is due to the dielectric relaxation of water molecules. Several models have been presented to model these dispersions. The simplest relaxation model is a called a Debye relaxation response and is formulated as:

$$\varepsilon = \varepsilon_\infty + \frac{\varepsilon_\infty - \varepsilon_s}{1 + j\omega\tau} \quad (3.35)$$

with  $\varepsilon_\infty$  and  $\varepsilon_s$  the high frequency and low frequency (steady state) limits of the permittivity and  $\tau$  the time constant of the relaxation. To account for the different relaxation mechanisms multiple first order terms can be summed, each representing a different relaxation mechanism.

### 3.3 Intra-oral environment

Biological tissue is a complex mixture of water, ions, membranes and macromolecules with different sizes and shapes. The elementary building block of all biological tissues is the cell, which can be specialised to perform specific functions. The cell is made of a protoplasm bound by a delicate membrane. The protoplasm contains proteins, polysaccharides, nucleic acids and lipids that are suspended in the intracellular water. The cells themselves are also suspended in water, called interstitial or intercellular water. The human body is composed of 50 - 70 % water, of which 67% is made of intracellular water, 25% interstitial water and 8% plasma[23].

Electromagnetic radiation originating from an intra oral device penetrates through the tissue structures of the oral cavity. An understanding of the intra-oral anatomy provides insights to the involved tissues and the best placement of the antenna.

Figure 3.5 illustrates a frontal view of the oral cavity , taken from [24].

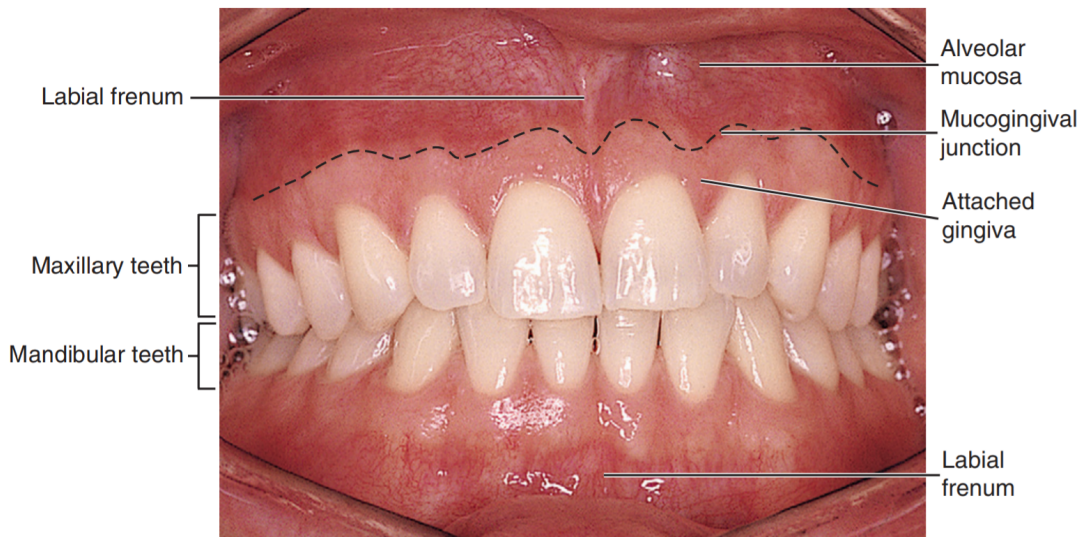


Figure 3.5: Annotated frontal view of the mouth. A thin antenna can be placed on the Labial frenum to be discrete. [24]

The moist lining of the oral cavity is called the oral mucus membrane or oral mucosa. No direct measurement of the dielectric properties of the oral mucosa is found in the literature, however this tissue shows some of the properties of skin and intestinal mucosa. In fact this similarity is well illustrated in figure 3.8 We use this similarity to approximate the dielectric properties of the oral mucosa to that of wet skin.

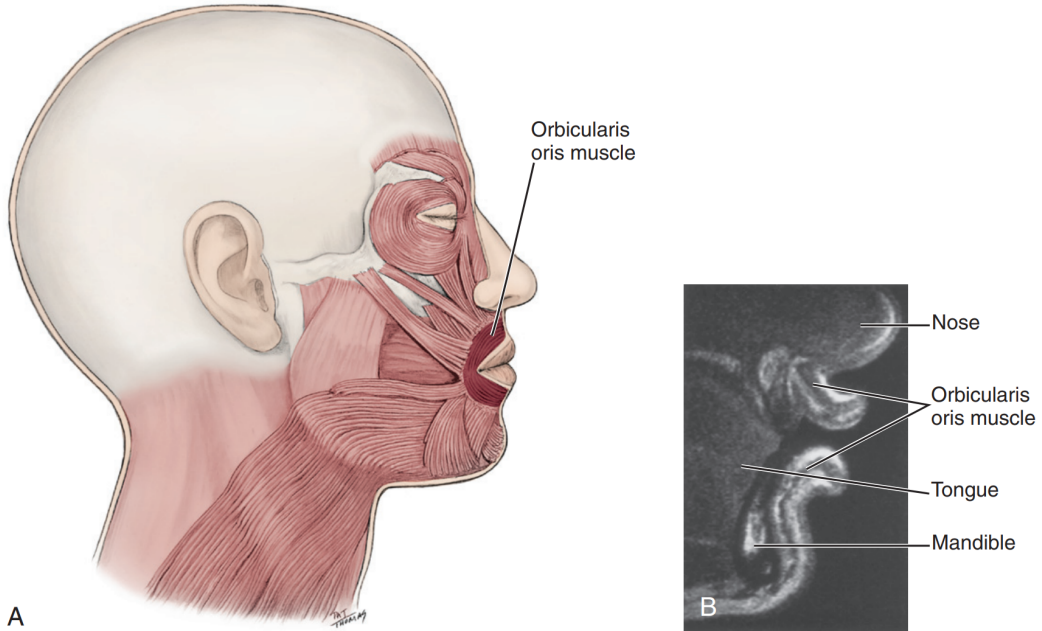


Figure 3.6: Figure A is side view the muscular structures of the face. For the selected antenna placement the main tissue responsible for electromagnetic absorption is the orbicularis oris muscle[24]

The dielectric properties of muscle, fat and skin 2440 MHz are illustrated in table 3.1

Table 3.1: Dielectric properties of tissues found in the oral cavity. The values are taken from <https://www.fcc.gov/general/body-tissue-dielectric-parameters>

Tissue	$\epsilon_r [F/m]$	$\sigma [S/m]$
Fat	5.28	0.10
Muscle	53.58	1.80
Skin dry	38.01	1.46
Skin wet	42.86	1.58

Of interest is the dielectric properties of saliva, as it surrounds the internal lining of the oral cavity and the potential intra oral antenna. [25]

### 3.4 Reflection at the interfaces

In addition to the absorption, electromagnetic waves are reflected at the interfaces between different structures. Additionally, an antenna does not radiate all the incoming power, it reflects a portion of the input power depending on its impedance and the impedance of the signal carrier. A transmission line model provides an understanding of these reflections.

Let's consider a simple electrical model of a sinusoidal voltage source  $V = V_0 \cos(\omega t + \phi_V)$  with phase  $\phi_V$ , angular frequency  $\omega$  and Amplitude  $V_0$  connected to a load  $Z$  via

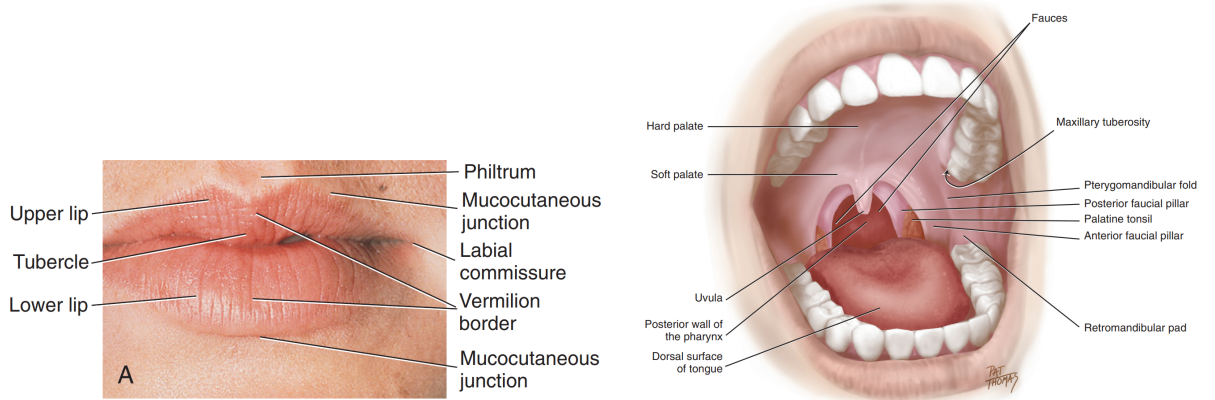


Figure 3.7: Figure A is side view the muscular [24]

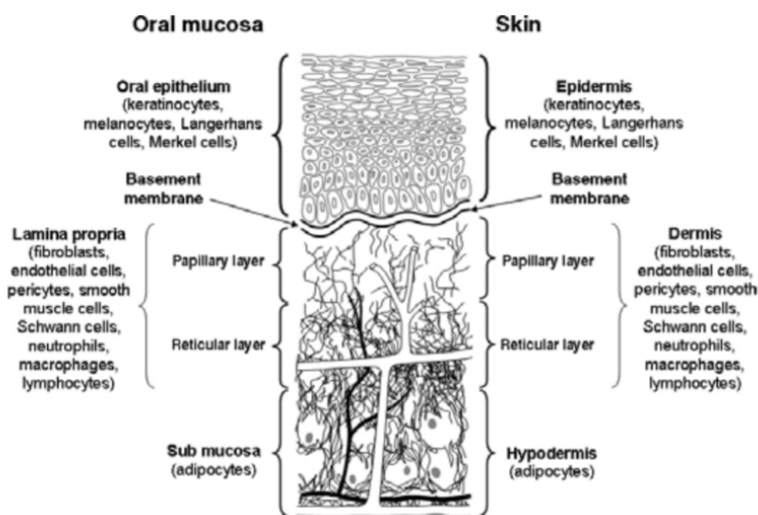


Figure 3.8: Comparison between the oral mucosa and the skin cavity[24]

conducting wires.

The voltage and current are always real quantities. However they are modeled as complex numbers in the form of  $\bar{V} = V_0 e^{j(\omega t + \phi_V)}$  and  $\bar{I} = I_0 e^{j(\omega t + \phi_I)}$  since working with exponential functions is much easier than fiddling with trigonometric identities. The observed Voltage and Current are then the real part of the respective complex quantity.

$$V = \Re\{\bar{V}\} = V_0 \cos(\omega t + \phi_V) \text{ and } I = \Re\{\bar{I}\} = I_0 \cos(\omega t + \phi_I)$$

This holds only for linear circuits , i.e. when only passive components are used, which is the case in this section.

The impedance  $Z$  is a complex number defined as :  $Z = R + jX$  , where  $R$  is the resistance and  $X$  is the reactance. $X$  is called an inductance when positive , and capacitance when negative.

Now let's consider an angular frequency  $\omega = 2\pi f = 2\pi 50Hz$  typically used for electric power supply. The corresponding wavelength of the signal traveling through

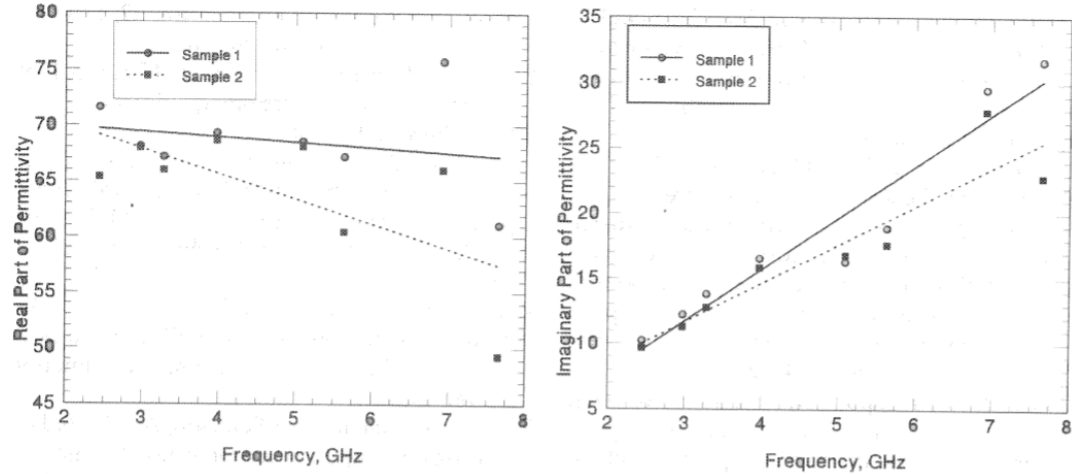


Figure 3.9: Real and Imaginary part of the complex dielectric permittivity of saliva ,  
Taken from[25]

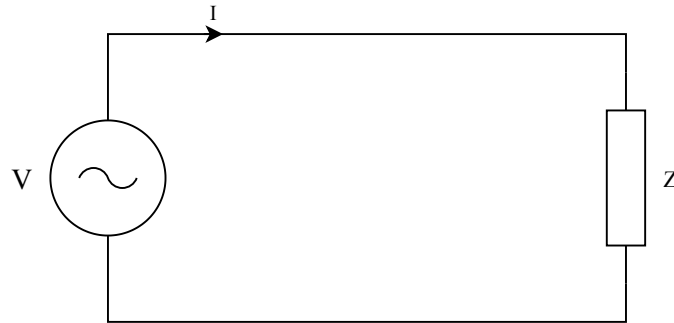


Figure 3.10: Radio system circuit

the conducting wires is  $\lambda = \frac{c}{f} = 6000\text{km}$ . The length of the conducting wire is much shorter than the wavelength and thus it can be assumed the the voltage and current across the line is constant.

However at higher frequencies this assumption no longer holds and the voltage and current along the transmission line are now functions of the distance from the source. This can be formulated using a transmission line model.

### 3.4.1 Transmission line model

A simple model of a two wire transmission line is introduced. We consider a short segment of length  $\Delta z$ , much smaller than the wavelength of interest. Each segment can be represented by circuit 3.11

The resistance  $R$  denotes resistance due to the finite conductivity of each conductor and has the unit  $[\frac{\text{ohms}}{\text{meter}}]$ . The inductance  $L$  denotes the total self-inductance of the two conductors and is measured in  $[\frac{\text{henries}}{\text{meter}}]$ . The capacitance  $C$  is due to the close proximity of the two conductors , and has the unit  $[\frac{\text{farads}}{\text{meter}}]$ .  $G$  is the conductance of

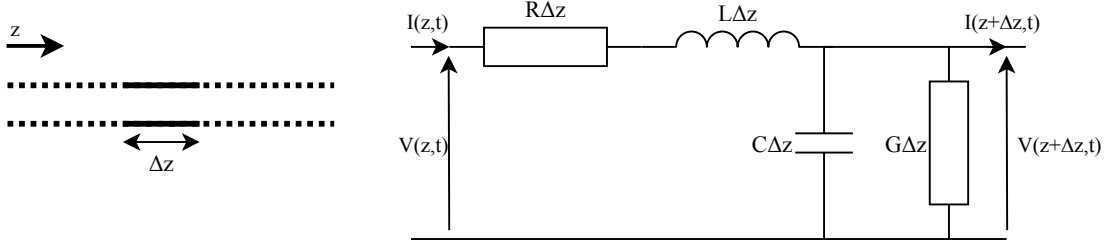


Figure 3.11: Two-wire transmission line

the dielectric material between the two conductors and have the unit [ $\frac{\text{siemens}}{\text{meter}}$ ].

Applying Ohm's law in the circuit 3.11 :

$$V(z + \Delta z) - V(z) = -(R + j\omega L) \Delta z \cdot I(z)$$

$$I(z + \Delta z) - I(z) = -(G + j\omega C) \Delta z \cdot V(z + \Delta z)$$

when  $\Delta z$  approaches zero, we obtain the differential form of the previous equations :

$$\frac{dV(z)}{dz} = -(R + j\omega L) \cdot I(z) \quad (3.37a)$$

$$\frac{dI(z)}{dz} = -(G + j\omega C) \cdot V(z) \quad (3.37b)$$

Differentiating with respect to  $z$  and combining both equations:

$$\frac{d^2V(z)}{dz^2} = (R + j\omega L)(G + j\omega C) \cdot V(z)$$

$$\frac{d^2I(z)}{dz^2} = (R + j\omega L)(G + j\omega C) \cdot I(z)$$

Defining  $(R + j\omega L)(G + j\omega C)$  as  $\gamma^2$  , where  $\gamma$  is called the propagation constant yields the wave equation for  $I(z)$  and  $V(z)$  :

$$\frac{d^2V(z)}{dz^2} - \gamma^2 V(z) = 0 \quad (3.39a)$$

$$\frac{d^2I(z)}{dz^2} - \gamma^2 I(z) = 0 \quad (3.39b)$$

Equation 3.39a and 3.39b are called the telegraph equations or transmission line equations , and they describe the voltage and current in a transmission line.

The propagation constant  $\gamma$  is complex valued and can be written as  $\gamma = \alpha + j\beta$ . We can solve for  $\alpha$  and  $\beta$  to obtain:

$$\alpha = \left[ \frac{1}{2} \left( \sqrt{(R^2 + \omega^2 L^2)(G^2 + \omega^2 C^2)} + (RG - \omega^2 LC) \right) \right]^{\frac{1}{2}} \quad (3.40a)$$

$$\beta = \left[ \frac{1}{2} \left( \sqrt{(R^2 + \omega^2 L^2)(G^2 + \omega^2 C^2)} - (RG - \omega^2 LC) \right) \right]^{\frac{1}{2}} \quad (3.40b)$$

### Solution to the telegraph equations

The traveling wave solutions to 3.39a can be found as [26]:

$$V(z) = V_0^+ e^{-\gamma z} + V_0^- e^{\gamma z} \quad (3.41a)$$

$$I(z) = I_0^+ e^{-\gamma z} + I_0^- e^{\gamma z} \quad (3.41b)$$

The term  $V_0^+ e^{-\gamma z}$  represents a forward propagating voltage in the  $+z$  direction, whereas the  $V_0^- e^{\gamma z}$  term represents a backward propagating voltage in the  $-z$  direction.  $V_0^+$ ,  $V_0^-$ ,  $I_0^+$  and  $I_0^-$  are complex constants, independent of time and position.

The ratio of the backward- to the forward propagating voltage wave is defined as the reflection coefficient of the transmission line in the position  $z$ :

$$\Gamma(z) = \frac{V_0^- e^{\gamma z}}{V_0^+ e^{-\gamma z}} = \Gamma_0 e^{2\gamma z}$$

where  $\Gamma_0 = \Gamma(z = 0) = \frac{V_0^-}{V_0^+}$

Inserting the equation 3.41a into 3.37a results into the following representation of the current on the line :

$$I(z) = \frac{\gamma}{R + j\omega L} (V_0^+ e^{-\gamma z} - V_0^- e^{\gamma z}) = I_0^+ e^{-\gamma z} + I_0^- e^{\gamma z}$$

The characteristic impedance  $Z_0$  can then be defined as:

$$Z_0 = \frac{V_0^+}{I_0^+} = -\frac{V_0^-}{I_0^-} = \frac{R + j\omega L}{\gamma} = \sqrt{\frac{R + j\omega L}{G + j\omega C}}$$

Unlike the voltage and current of a transmission line, the characteristic impedance does not depend on the position  $z$ . We use the characteristic to define a normalized incident

and scattered voltage waves:

$$a(z) = \frac{V_0^+ e^{-\gamma z}}{\sqrt{Z_0}} \quad (3.42a)$$

$$b(z) = \frac{V_0^- e^{+\gamma z}}{\sqrt{Z_0}} \quad (3.42b)$$

We consider a terminated transmission line with a load impedance  $Z_L$  as represented, the Two-port network in figure 3.12 can be modeled using the normalized and scattered incident voltage waves.

As seen in the previous section, a forward and backward propagating wave exist on a transmission line. Several matrices can be used to model the current and voltage relationship of a given network, for example the impedance “Z-parameters” or the admittance “Y-parameters” matrices. At low frequencies these parameters can be rapidly measured using short and open circuits tests at the terminals. At microwave frequencies ideal open and short circuits configurations are difficult to implement.

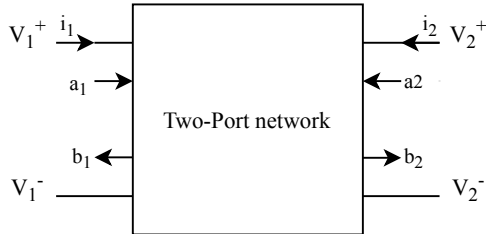


Figure 3.12: Two-port network

### 3.5 Quality metrics for wireless links

A typical wireless architecture is illustrated in figure 3.13 .

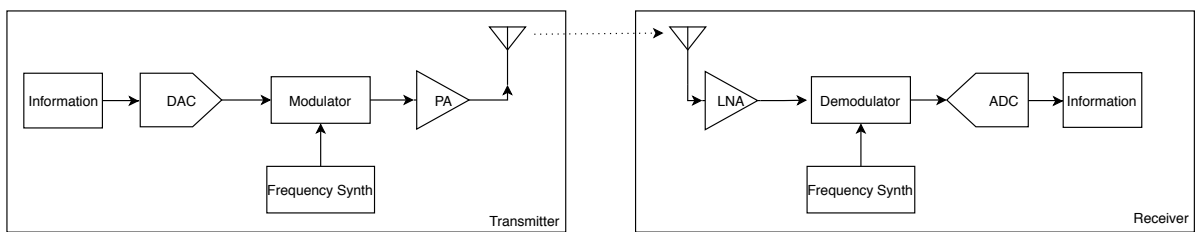


Figure 3.13: Typical wireless structure

From a system point of view, a wireless link can be assessed by the rate of successfully transmitted bits of information and the power consumed by the transmitter. In this

work we use a systematic evaluation of the However a proper evaluation of the quality of a wireless link requires the discussion of its spatial and temporal characteristics.

Several works demonstrated that the transmission of a low powered transmitter is not isotropic, i.e. the transmitter has a circular range in which packets are received equally. This anisotropy results in radio irregularities that can be explained by device and propagation media properties. Device properties include the directivity of the antenna, the sending power, receiver sensitivity and the Signal-Noise Ratio [27]. Propagation media properties include the background noise and the environmental effects resulting in constructive and destructive interference. The major cause of radio irregularity can be explained by the variance in signal path loss due to the reflection, diffraction and scattering of the radio signal.

A thorough survey of the metrics typically used to qualify wireless links is presented in [28]. In this work the wireless link was qualified by means of the Received Signal Strength Indication (RSSI), Received Packets per Second and a simulation of sensor values that are validated at the receiver.

# 4 Methods

## 4.1 Design Considerations

Several considerations must be taken into account for implementing a wireless link from inside the mouth cavity. The main consideration is the total size of the device. Any intra-oral device should be as thin as possible to be ergonomic and not to interfere with regular speech and breathing activities. This poses restrictions to the available antenna and battery sizes. A smaller antenna inherently performs worse than a large antenna leading to a lower efficiency and higher power consumption. The wireless link should be robust against head movement in nominal conditions. Since the device is to be used to control a mouse cursor, lost packets are easily perceived as an unresponsive cursor leading to a less ergonomic experience. Finally since the device is to be battery operated, a sufficiently large battery life should be targeted.

### 4.1.1 Antenna

Several antennas types were considered for this implementation. A distinction of two types can be made. Embedded antennas can be directly integrated in the transceiver PCB. In this category we find ceramic antennas and PCB trace antennas as illustrated in figure A. The main advantage of using an embedded antenna is the smaller size of the complete system. However these antennas are highly dependent on the ground plane size and shape. Additionally tuning an embedded antenna requires modifying the impedance matching network or modifying the physical shape in the case of the PCB antenna. This results in a more complex tuning process as a new PCB should be printed for every iteration. Finally characterizing an embedded antenna is more complex as the antenna can not be separated from the rest of the system.

An external antenna connects to the transceiver through a coaxial cable which allows a more flexible placement of the antenna in the mouth cavity. Additionally an external antenna can be separately tuned for operation inside the mouth cavity and then easily connected to the transmitter. The iterative process of tuning the antenna can then be done independently of the rest of the system, and finally the tuned antenna can be easily swapped in the final system.

Following this consideration it was decided to use an external antenna. The smallest available antenna in the 2.4 GHz was selected to provide a baseline for the achievable performance. It is expected that an off the shelf antenna is not optimized for an intra-oral operation, however the goal of this feasibility analysis is to determine how much would this affect the wireless link.

For an active transmitter the first design criterion is the frequency band of operation. Lower frequencies penetrate more easily through human tissues. However smaller antennas have better radiation in higher frequencies. The deciding factor for choosing Surveying off the shelf antennas and transceivers, the frequency band of 2.4 GHz is selected for several factors.

#### 4.1.2 Power

The power discussion provided in this part is a crude analysis that attempts to define an upper limit power constraint for the transceiver.

The transceiver is to be battery operated. Smaller batteries adequate with the size requirements defined tend to have a smaller capacity. Table is an overview of small rechargeable and commercially available Li-po batteries.

Table 4.1: Overview small batteries

Battery	Pdbattery PD252020	Data Power DTP301120	LiPol Battery LP152517	LiPol Battery LP072736	LiPol Battery LP044823
Thickness[mm]	2.5	3	1.5	0.7	0.4
Width[mm]	20	11	25	27	25
Length[mm]	22	20	17	36	29
Capacity[mAh]	60	40	50	25	7.5
Voltage[V]	3.7	3.7	3.7	3.7	3.7
Technology	LiPo	LiPo	LiPo	LiPo	LiPo

A battery size of 50 mAh will be set as the maximum battery size. We can now define an arbitrary target battery life of 5 hours. With this value a maximum load current can be calculated as  $50 / 5 = 10$  mA. The power is shared by the sensors, the transmitter and the SoC. To define a maximal current consumption of the RF module , it is relevant to compare some sensors:

We can define 2 mA as the maximum current consumption for the sensors. With this consideration the maximum power consumption of the RF module and the SoC is 8 mA.

Table 4.2: Common sensors power consumptionSources :  
<https://www.melexis.com/en/product/MLX92213/MicroPower-Low-Voltage-Hall-Effect-Latch#> , <https://www.st.com/resource/en/datasheet/lis3dh.pdf>  
[https://dammedia.osram.info/media/resource/hires/osram-dam-2496568/SFH\\_7779\\_\(IR-LED+\\_proximity\\_sensor+\\_ambient\\_light\\_sensor\).pdf](https://dammedia.osram.info/media/resource/hires/osram-dam-2496568/SFH_7779_(IR-LED+_proximity_sensor+_ambient_light_sensor).pdf)

Sensor	Osram SFH7779	STMicroelectronics LIS3DH	Melexis MLX92213
Type	Infrared proximity sensor	Accelerometer	Hall effect magnetic sensor
Average current consumption [ $\mu A$ ]]	263	185	48
Voltage [V]		3V	3V
Conditions	ILED = 100 mA trep_PS = 100 ms	Sampling rate 1344 Hz , resolution 12 bit.	

## 4.2 Implementation

The implementation of the evaluation prototype is organized in Figure 4.1:

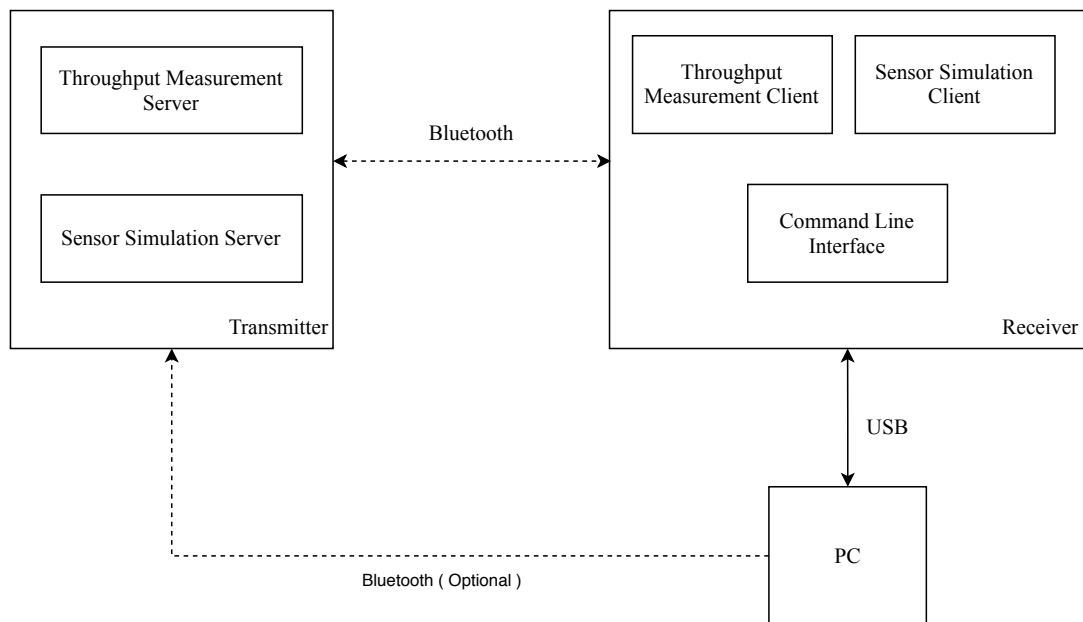


Figure 4.1: Overview of the transmitter structure

- Transmitter: implements a simulation of sensor data, a wireless command line interface to set the transmission configuration and integrates a throughput measurement service.
- Receiver: implements the clients interfacing the services provided by the transmitter and a wired command line interface to the computer providing an access to the received data and a possibility to remotely configure the transmitter.
- PC: Implements an application for data acquisition and visualisation.

Table 4.3: Overview BLE SiP solutions

Module	TAIYO YUDEN EYSHSNZWZ	U-blox ANNA-b112	Panasonic PAN1740A	Panasonic PAN1780	Würth Electronics Proteus-III
SoC	nRF52832	nRF52832	DA14585	nRF52840	nRF52840
$I_{Transmit}$ [mA]	7.5 @ +4dBm - DCDC	5.3 @ +0dBm -DCDC	4.9 @ +0dBm -DCDC	4.8 @ +0dBm	6.4 @+0dBm
Voltage [V]	1.7 -3.6	1.7 - 3.6	1.8-3.3	1.7 - 5.5	1.8 - 3.6
Antenna type	PCB trace	Ceramic chip antenna - Pin	Ceramic chip antenna	Ceramic chip antenna	Ceramic chip antenna - Pin
Max radiated output power [dBm]	6	5 / 9 internal / external antenna	0	8	4/6 internal / external antenna
BLE qualification	5.0	5.0	5.0	5.0	5.1
ADC		12 bit -8 channel	10 bit 4 channel		
GPIO		25	12		
Size [mm]	3.25 x 8.55 x 1.00	6.50 x 6.50 x 1.20	9.00 x 9.50 x 1.80	15.00 x 8.70 x 2.10	12.00 x 8.40 x 2.00
++	smallest	certified with flexible antennas	2 integrated Crystal Oscillators	2 integrated Crystal Oscillators	Castellated pins

#### 4.2.1 Transmitter

The transmitter uses the u-blox BMD-341 System in Package (SiP). This SiP includes the nRF52840 SoC and the required components for stand-alone operation. The SiP provides a U.FL connector to an external antenna. The used external antenna is the Taoglas FXP.75 Atom.

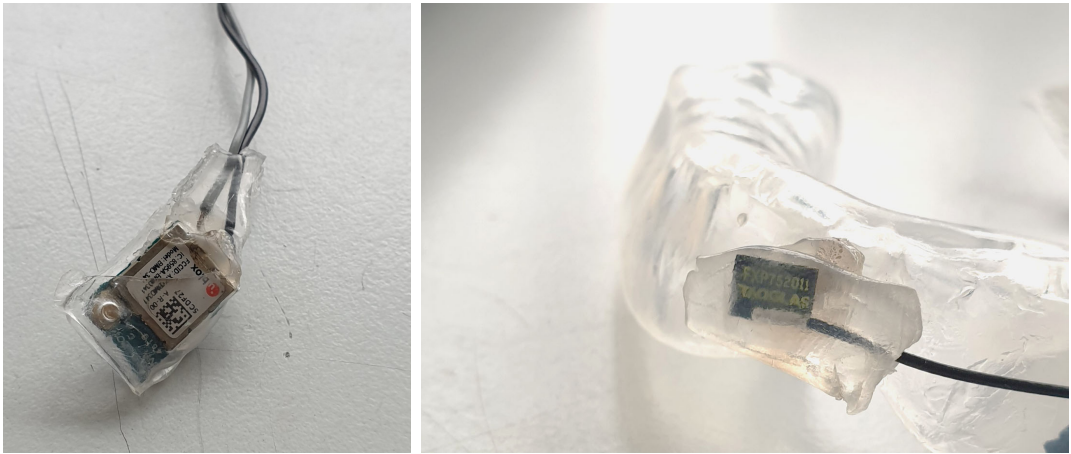


Figure 4.2: The antenna is sealed with a radome to eliminate the effects of saliva . A Ufl to SMA cable connects the antenna to the network vector analyzer.

The transmitter is programmed using the SWD debug interface. The used debugger is the development kit nRFDK52 and connects to the transmitter according to the wiring in figure. The SiP provides two configurations for powering the system. The first is the High Voltage mode that is activated when connecting VDDH to the power supply. At VCC a regulated 3.0 V output is provided for external sensors. The second mode the low voltage mode and is selected by connecting VCC and VDDH to the power supply.

## Programming

The evaluation prototype is programmed to provide a throughput measurement and sensor simulation services. The connection parameters can be modified at runtime through a custom command service.

To program the transmitter the Software Development Kit (SDK) of the manufacturer is used. The SDK provides a wide range of examples showcasing the usage of the different peripherals of the system. The programmed application is based on the ATT\_MTU\_TEST provided in the SDK 15.0.03. This application demonstrates the usage of the command line interface, the Bluetooth stack and the USB interface to implement the throughput measurement routine.

The programming is done using the Segger Embedded Studio IDE and in the C Language.

The sensor data is simulated in 3 int16\_t values, each incremented in a predefined way to enable sequence validation in software. A configurable delay value: delayTX is waited before sending new data via the BTS server. The BTS server is a custom Bluetooth service that implements the sensor simulation service and the configuration exchange service. The main loop of the transmitter is illustrated in figure 4.3. The transmitter expects connection and configuration events. A connection event is fired

when the transmitter is advertising and an the receiver is scanning or vice versa. Once a connection event is fired the transmitter discovers the services exposed by the receiver and vice versa. The implementation sees no difference between the receiver and the transmitter. The only difference is that the logging and usb modules are deactivated on the transmitter to save power.

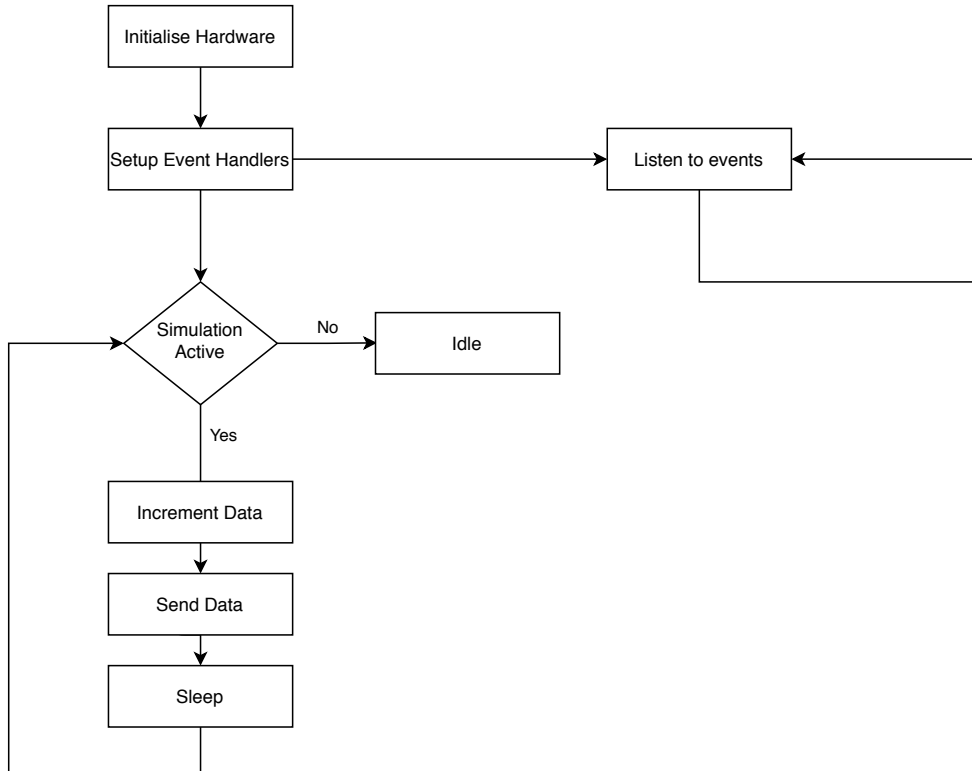


Figure 4.3: Transmitter main loop

#### 4.2.2 Receiver

Two possible receiver configuration are used as illustrated in figure . In the first configuration the embedded Bluetooth low energy device of a laptop is used. In the second configuration the nrf PCA10059 board is used. This board is based on the nRF52840 SoC and connects to a PC through USB. Several advantages arise from using a custom receiver. The receiver position can be flexibly set in the proximity of the user. Additionally the connection parameters can be ensured to be optimal for either power consumption, speed or range. With an embedded receiver the possible configurations are limited and vary from laptop to laptop.

The receiver program implements the clients to communicate with the servers present in the receiver, and a command line interface to remotely configure the transmitter.

```

COM13
Commander: resize
Commander: clear
Commander:
SendCMD      Set_Mode      StartTT
Timer_test   ToggleLED   TrhoughputTest
about        adv          app_size
balloc       clear         cli
config       dis           error
flashlog    history       log
log_msg     print         reset
resize      run            scn
start       stop           sync
task_manager txset
Commander: config print
===== Current test configuration =====

Board role:          not selected
ATT MTU size:        247
Data length:          251

```

```

COM12
<info> app: BTS Client Initialized.

<info> app: Starting advertising.

<info> app: Connected as a peripheral.

<info> app: Discovering GATT database...

<info> app: Sending PHY Update, 2 Mbps.

<info> app: Data length updated to 251 bytes.

<info> app: ATT MTU exchange completed. MTU set to 247 bytes.

<info> app: PHY update accepted. PHY set to 2 Mbps.

<info> app: AMT service discovered at peer.

<info> BTS_CLIENT: BTS service discovered at peer.

<info> BTS_CLIENT: CMD_BLE_UUID Handle assigned.

```

Figure 4.4: Receiver Control Interface. Top window is The command line interface COM port, Bottom is the output COM port

### Command Line Interface

The receiver provides a command line interface to interface with the transmitter. This is implemented as a virtual COM port over USB and can be accessed using a serial terminal software such as Putty. A second virtual COM port provides access to the logging output, where the received data and other debugging information can be viewed. Figure 4.4 illustrates the receiver interfaces.

Table 4.5 illustrates the required commands to reproduce the measurements.

## Configuration synchronisation

To wirelessly modify the transmitter's configuration a simple command structure is implemented. A command packet contains an opcode specifying the command type and a data structure containing the command data. This interface is used to adjust the simulated sensors update during runtime.

### 4.2.3 Data acquisition and visualisation

To acquire the data from the evaluation prototype, a python tool is implemented. This tool interfaces with the evaluation prototype over internal Bluetooth interface or via the custom receiver connected through USB. This tool captures the received data in a FIFO buffer, and extracts and plots several metrics.

#### Used libraries

The used libraries are illustrated in table 4.6.

Table 4.6: Wireless Quality Tool Used Libraries

Library	Version	Description
PyQt5	5.15.1	user interface
PyQtGraph	0.11.0	plotting
pickle5	0.0.11	saving/restoring measurement buffer
bleak	0.9.0	GATT client
asyncio	3.4.3	async/await syntax for python
pyserial-asyncio	0.4	connect to serial ports using asyncio

#### User Interface

The used interface is illustrated in figure ??.

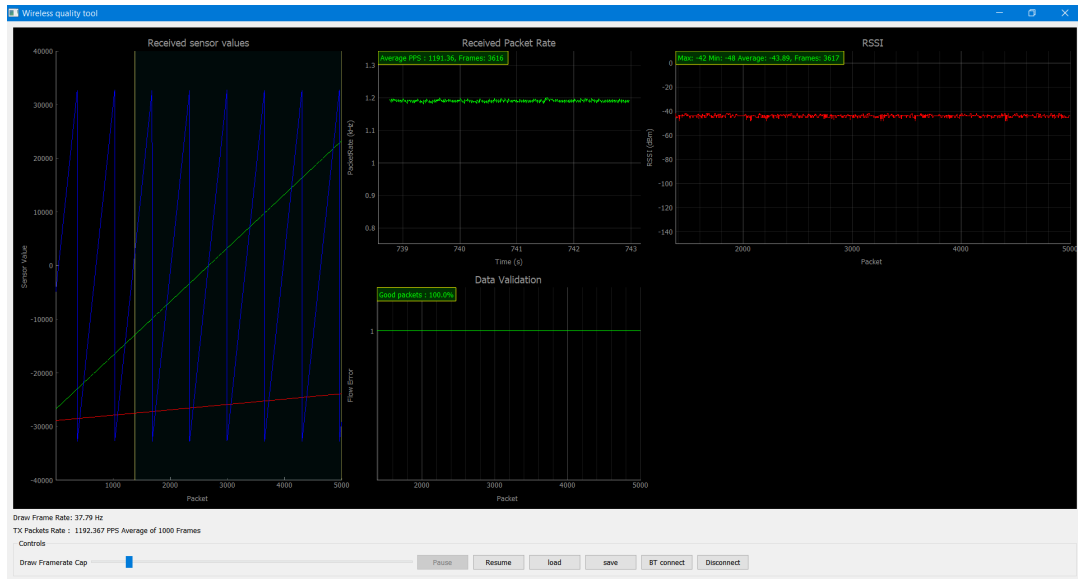


Figure 4.5: Wireless Quality Tool GUI

The first plot is the received simulated sensor values. A region selector selects the frames that are analysed in the other plots. The selected region is validated against the transmitter sequence to detect the dropped packets. The data validation plot visualises the rate of good packets in the selected region.

The received packet rate plot visualises the the rate of received packets per second. The RSSI plot visualises the measured rssi from the transmitter. This plots is only available when using the custom receiver.

The drawing frame rate cap can be adjusted. This can be required for slower computers to ensure that the drawing does not bottleneck the data acquisition. The user interface provides controls for pausing/resuming the plotting, loading/saving the data buffer and connecting/disconnecting using the internal Bluetooth interface. The custom receiver is interfaced via a serial connection.

Table 4.4: Overview BLE SoC solutions

Module	Renesas RX23W	nRF52840	Dialog DA14585	Cypress CYW20721	Texas CC2640R2L	STM32WB55CEU6
$I_{Transmit}$ [mA]	4.3 at +0dBm 8.7 at +4dBm	4.8 at +0dBm 9.6 at +4dBm 14.8 at +8dBm	3.4 at +0dBm	5.6 at +0dBm	6.1 at +0dBm 9.1 at +5dBm	5.2 at +0dBm
RF connection	RF single I/O	RF single I/O	RF single I/O	RF single I/O	Single-ended or differential	RF single I/O
Voltage [V]	1.8 - 3.6	1.7 - 5.5	1.5-3.0	1.76 - 3.63	1.8 - 3.8	1.71 - 3.6
Max output power [dBm]	6	8	0	5	5	6
BLE qualification	5.0	5.1	5.0	5.0	5.1	5.0
ADC	14 channel 12 bit	8-channel 12 bit	4 channel 10 bit	28 channel 13 bit	8 channel 12 bit	13 channel 12 bit
GPIO	56	48	25	16	31	30
Size [mm]	7 x 7	7 x 7	5 x 5	5 x 5	7 x 7	7 x 7
Power	On-chip DC-to-DC converter or linear regulator	On-chip DC/DC buck converter	On-chip DC/DC Buck/-Boost	On-chip internal DC/DC converter	Linear voltage regulator	companion chip for matching MLPF-WB55-02E3
++	On-chip matching circuit	High output power	lowest current consumption	Differential antenna pin		

Table 4.5: Command Line Interface Commands

---

Command	Description
init	Initialises the implemented Bluetooth services
config	modifies the configuration of the connection parameters.
<subcommand>	Pressing TAB shows possible sub-commands.
txrate <value>	set the delay in the transmission loop to the value, in $\mu s$
start / stop	start / stop sensor simulation
measureTP	measures the throughput
adv	start advertising
scn	start scanning
dis	disconnects
sync	synchronizes the connection parameters with the transmitter

---

# 5

## Chapter 5

# Measurements

### 5.1 Radiation pattern

Description : Antenna placed on tripod with adjustable height and orientation. Test subject wears dental retainer and sits on a rotating chair at distance d from receiver. The angle of the rotating chair is measured using a smartphone placed on the armrest of the chair.

Measurement : Capture received data using the wireless quality tool.

### 5.2 Throughput measurement

The throughput measurement routine is illustrated in figure 5.1. The test is started and configured via receiver command line interface.

### 5.3 Signal strength measurement

The custom receiver provides a Received Signal Strength Indicator measurement with a 1dB resolution[29].

### 5.4 Packets per Second

The number of packets per Second (PPS) is measured. Only valid packets are counted since data integrity and flow control happen on the link layer. The ratio of  $\frac{PPS}{PPS_0}$ , where  $PPS_0$  is the measured value outside the mouth, provides a measure for the rate of corrupted packets.

### 5.5 Validation

Each received packet is validated using the known transmitter sequence. The packet where the sequence is broken is marked as invalid. Invalid packets occur when packets

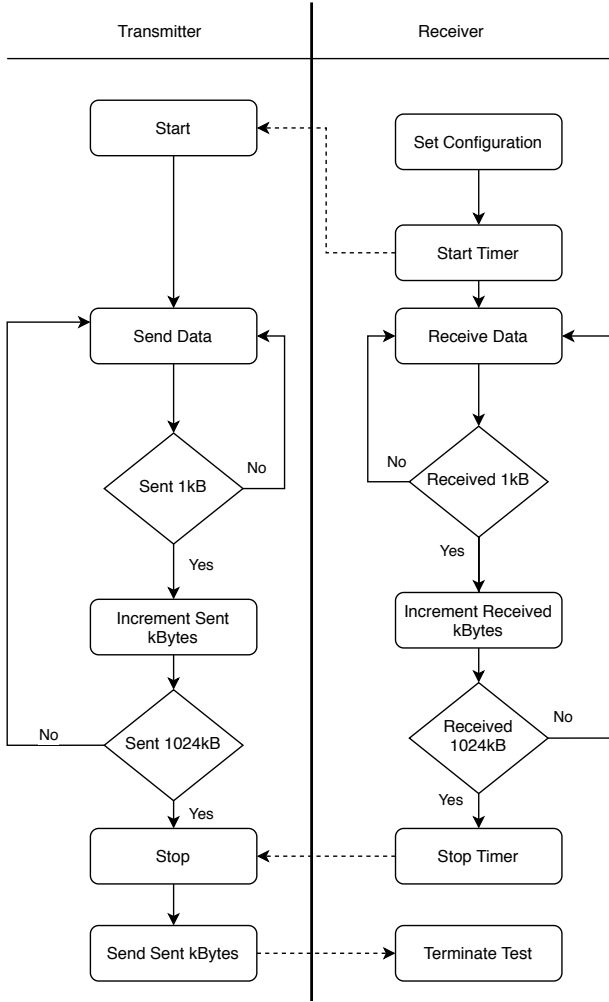


Figure 5.1: Throughput measurement routine.

are dropped. When a packet fails the flow control and integrity checks in the link layer, it is retransmitted. The retransmission timeout specifies how long the transmitter tries to retransmit a packet. Lowering the polling rate increases the chance of a packet being successfully sent, as the transmitter has more time for retransmission.

## 5.6 Antenna Performance

The antenna is covered with a bio-compatible radome to prevent the antenna from getting wet. Additionally the antenna is attached to a dental retainer to have a fixed position between measurements. Figure 5.2 illustrates the mounting of the antenna on the dental retainer. To eliminate the effects of interference antenna measurements are performed in an anechoic chamber.

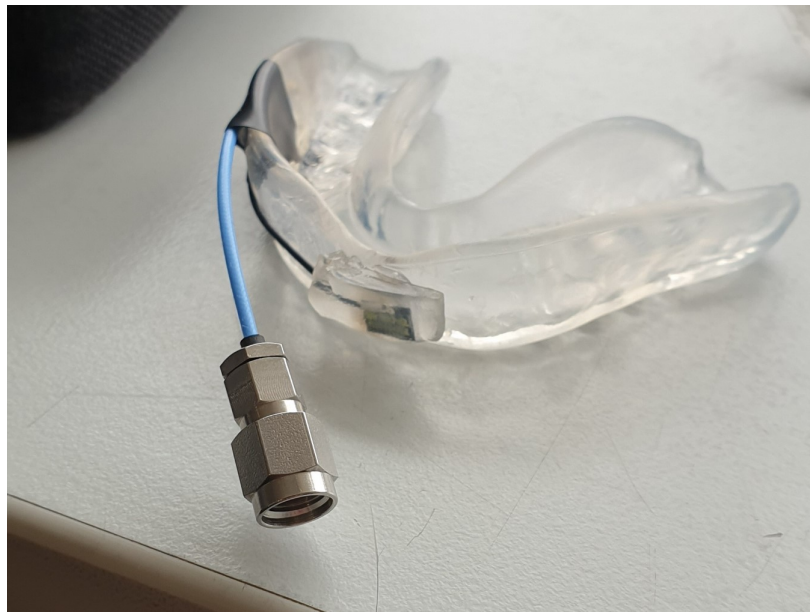


Figure 5.2: The antenna is sealed with a radome to eliminate the effects of saliva .A Ufl to SMA cable connects the antenna to the network vector analyzer.

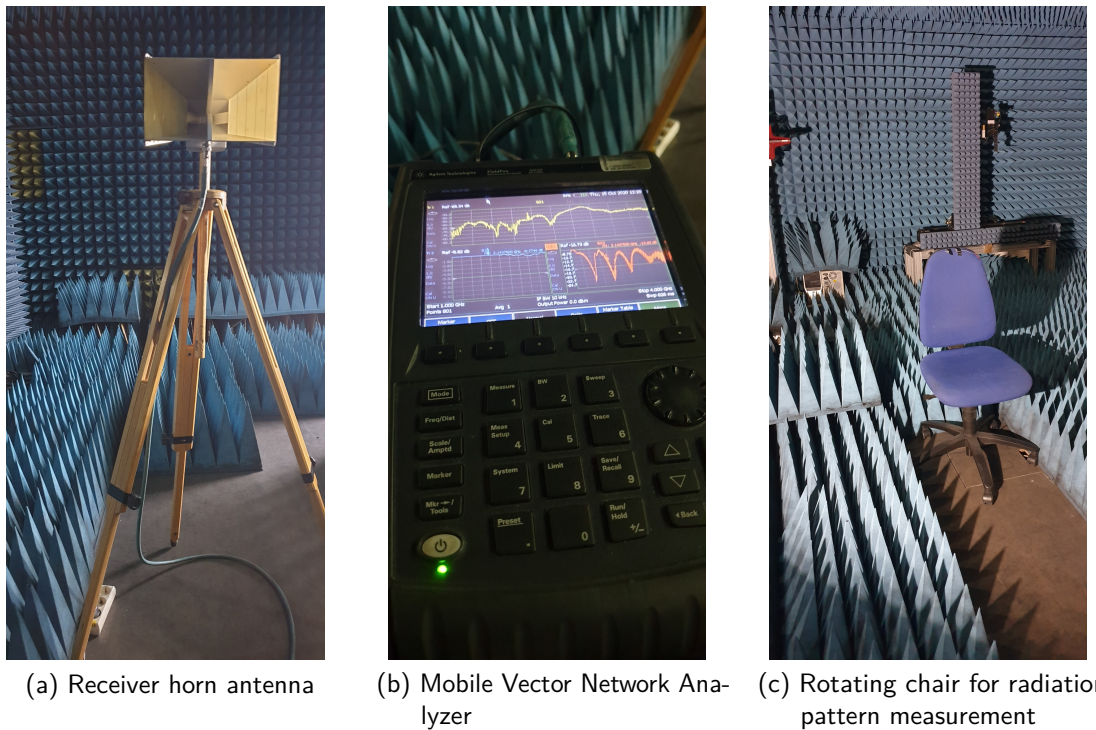


Figure 5.3: Radiation Pattern Measurement configuration. Measurement configuration:  
-Receiver placed 1m away from rotating chair.-Test subject wears dental retainer, keeps stable head orientation.-Vector Network Analyzer connects to receiver and transmitter.-Calibration-Chair is rotated from -90 to 90 degrees, measurement each 15 degree.

The measurement was performed with vertical and horizontal polarized antenna config-

uration as illustrated in 5.4.



(a) Vertical polarization configuration



(b) Horizontal polarization configuration

Figure 5.4: Radiation Pattern Measurement configuration. Measurement configuration:  
-Receiver placed 1m away from rotating chair.-Test subject wears dental  
retainer, keeps stable head orientation.-Vector Network Analyzer connects  
to receiver and transmitter.-Calibration-Chair is rotated from -90 to 90  
degrees, measurement each 15 degree.

Throughput measurements configurations

# 6 Chapter 6 Evaluation

The evaluation is divided in two part. The first part is the antenna evaluation, in which the reflection coefficient and the radiation pattern of the antenna is measured. The second part is an evaluation of the complete radio system with the antenna, in which several metrics are measured that help quantify the quality of the wireless system.

## 6.1 Antenna performance

Materials in close proximity to the antenna influence its impedance and its reflection coefficient. Several measurements are performed to document this effect. Table 6.1 describes the test configurations.

Table 6.1: Antenna evaluation configurations

Configuration	Description
A	antenna out of the box, placed over a Styrofoam plate
B	antenna out of the box, inserted inside the mouth
C	antenna coated with protective radome, attached to dental retainer and worn by test subject
D	antenna out of the box, pressed between two fingers

This was observed when the antenna is coated with saliva or is mounted inside the dental retainer. Figure6.1 illustrates some measured values.

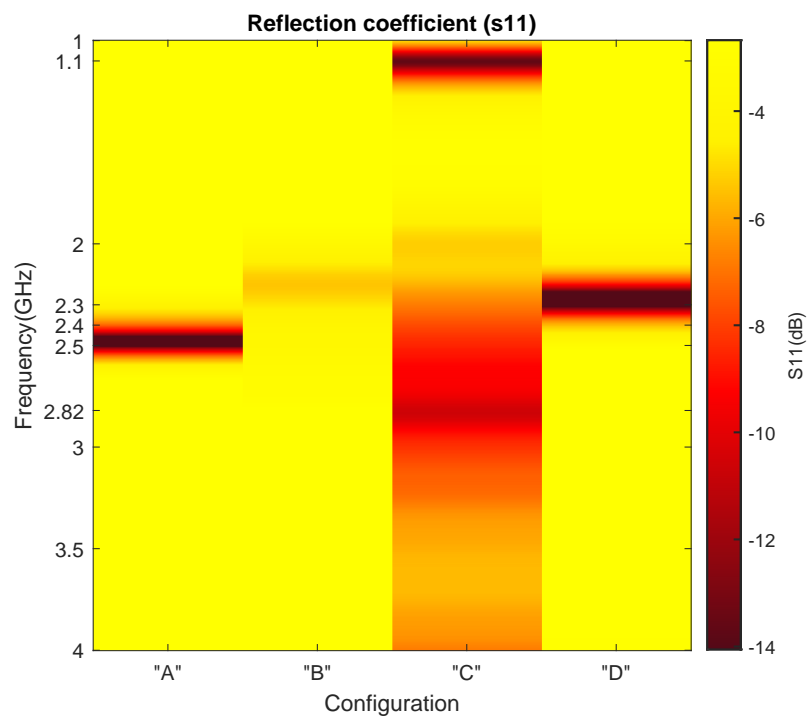


Figure 6.1: Measured S11 of the antenna under various configurations. In the absence of a matching network, the antenna is easily detuned in proximity to body tissues.

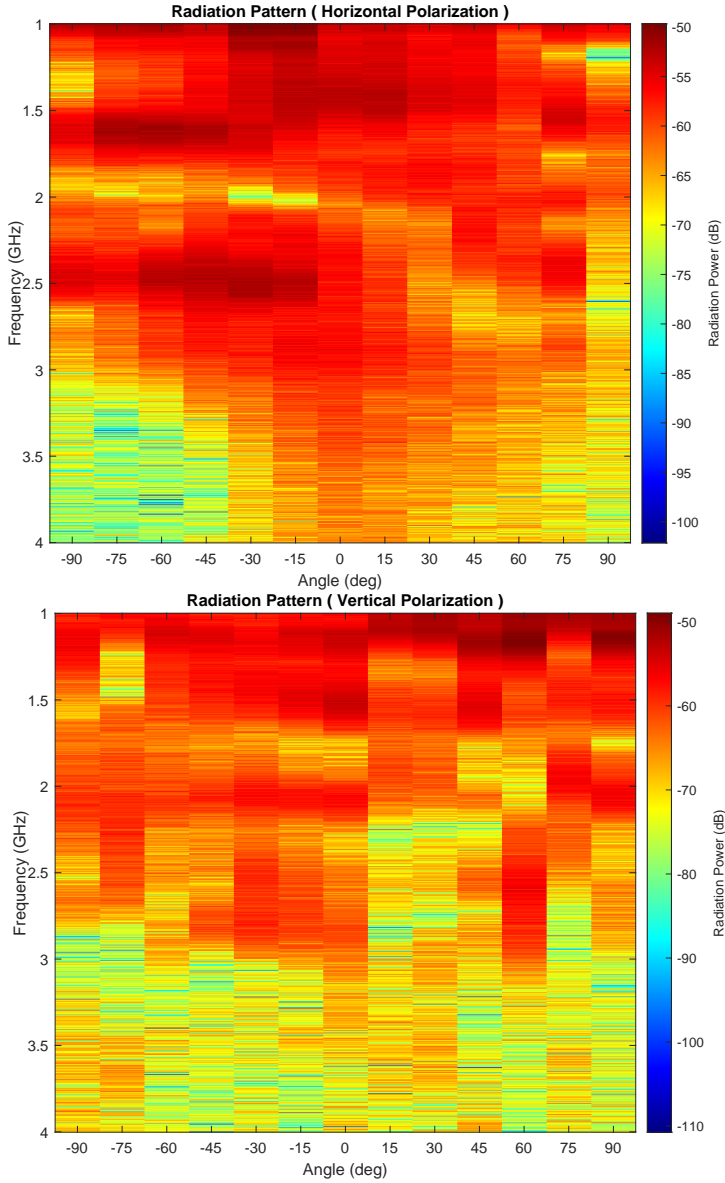


Figure 6.2: Radiation Pattern.

The radiation pattern shows that the radiation power is not symmetrical. This is expected due to the placement of the antenna connector on only one side of the dental retainer. For the frequency range of interest : 2400-2480 MHz, maximal radiation power is observed at the antenna connector side between -45 and 0 degrees for horizontally polarized waves. The vertical polarized measurement shows that the antenna is not vertically polarized.

### 6.1.1 Reflection coefficient

Figure 6.3 illustrates the measured reflection coefficient. In the first figure a difference between the two figures is noticed, even though the reflection coefficient does not depend on the polarization of the antenna. The dental retainer was removed between

the two measurement. The connecting cable orientation and the head orientation could have changed between the measurements. It can be concluded however that the used antenna with its protecting radome are not optimized for intraoral usage. Even though it can still be usable under certain configurations.

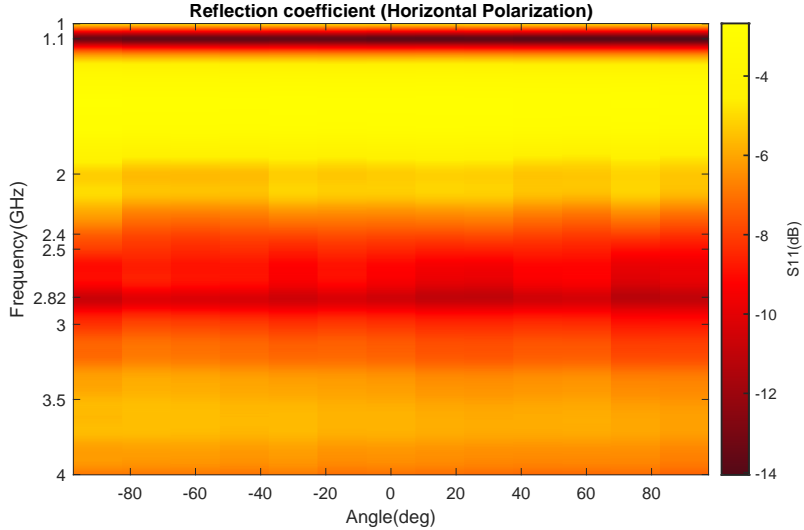


Figure 6.3: Radiation Pattern.

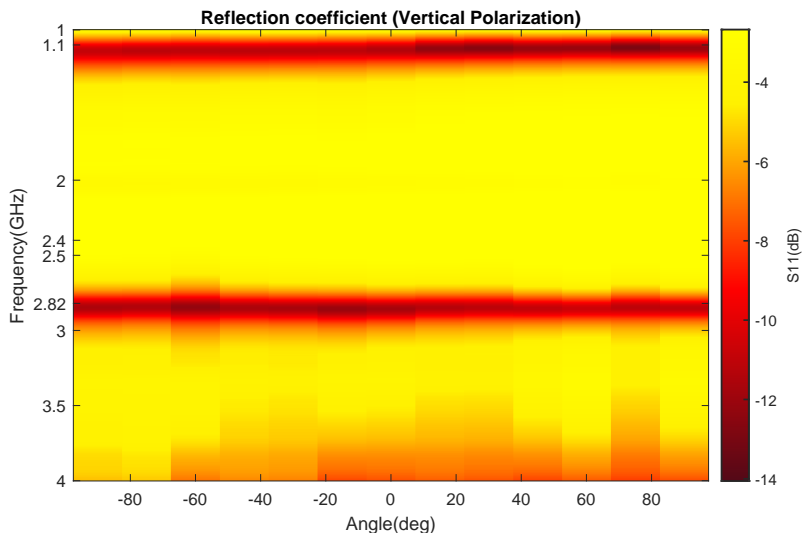
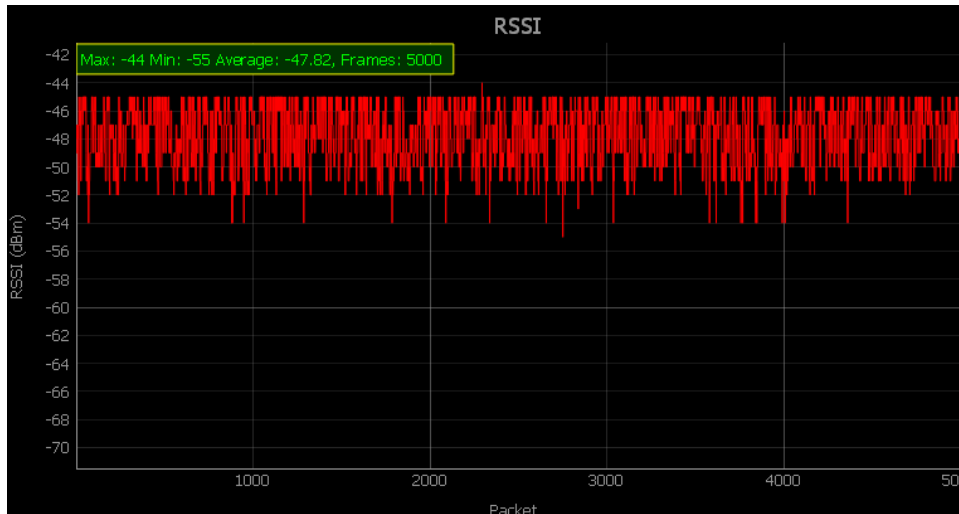


Figure 6.4: Radiation Pattern Vertical.

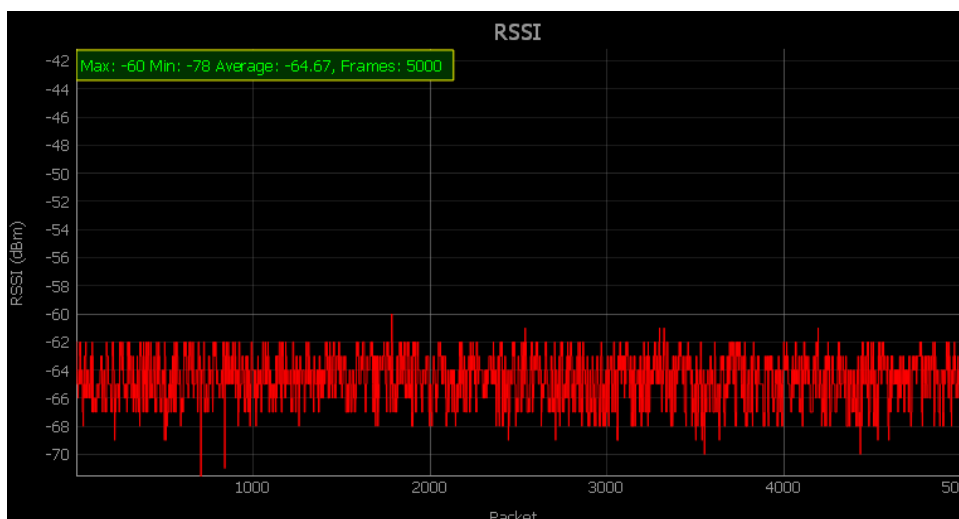
## 6.2 Radio system performance

### 6.2.1 Radiation pattern

In the first test case the impact of inserting the transmitter inside the is evaluated. Figure 6.5 illustrates the measured RSSI value inside and outside the mouth at a distance of 50cm.



(a) Transmitter in front of the mouth



(b) Transmitter inside the mouth

Figure 6.5: Measured RSSI value for the transmitter placed 50 cm in front of the receiver

When the transmitter is placed in front of the mouth, we calculate an average value of -47.82 dBm with a standard deviation of 2.1 dBm. When the transmitter is placed inside the mouth the average RSSI value is lowered to -64.67 dBm with a standard deviation of 1.63 dBm. A lower Average value is expected due to the absorption of the electromagnetic radiation by the mouth tissues. The lower standard deviation for the values inside the mouth can be explained by the fixed position during the measurement inside the mouth, contrary to the measurements in front of the mouth with transmitter held by hand.

The received packets per second did not vary between the two measurements, at 666 packets per second. This indicates that no packets are lost. This is confirmed by the measured data validation metric reporting 100% good packets in both cases.

The above measurements are repeated at different angles to obtain the radiation pattern

at 50 cm in figure 6.6. Every measurement point represents the average of 5000 frame.

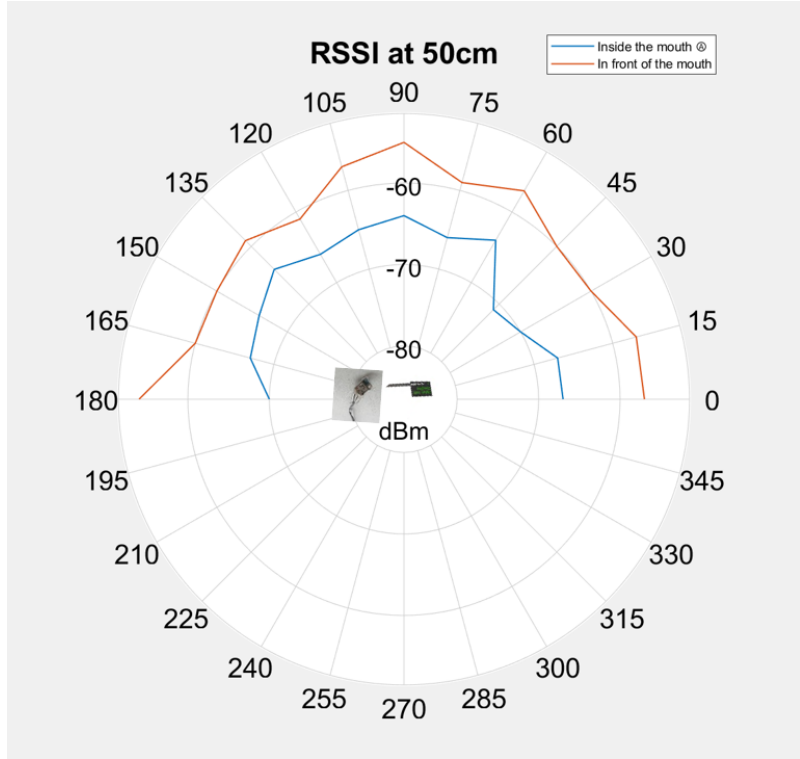


Figure 6.6: Radiation pattern measured using the RSSI value in a typical usage environment

We notice that the measured radiation pattern of the complete evaluation prototype differs from the radiation pattern of the antenna measured in 6.2. Several factors can explain this behavior. The extension cable used when characterizing the antenna is replaced by the transmitter and the ufl connector present in the PCB which leads to a difference in measured directivity.

Measuring the RSSI outside an anechoic chamber results in several uncertainties. External radiation from other devices operating in the 2.4 GHz band could not be avoided. Additionally the transmitted signal reflects over the walls and the other structures of the room. These reflected signals interfere both constructively and destructively giving rise to a spatial distribution of the RSSI value that does not depend only on the antenna. However we can still observe in all measured distances the presence of spots with high signal intensity. Using the visualization tool we can identify such locations easily by observing the real time validation and signal strength plots.

### 6.2.2 Data rate

The achieved wireless data rates are illustrated in figure 6.7. We observe that the achieved data rate is lowered when the evaluation prototype is inserted inside the mouth. This is the result of the time spent re-transmitting lost packets.

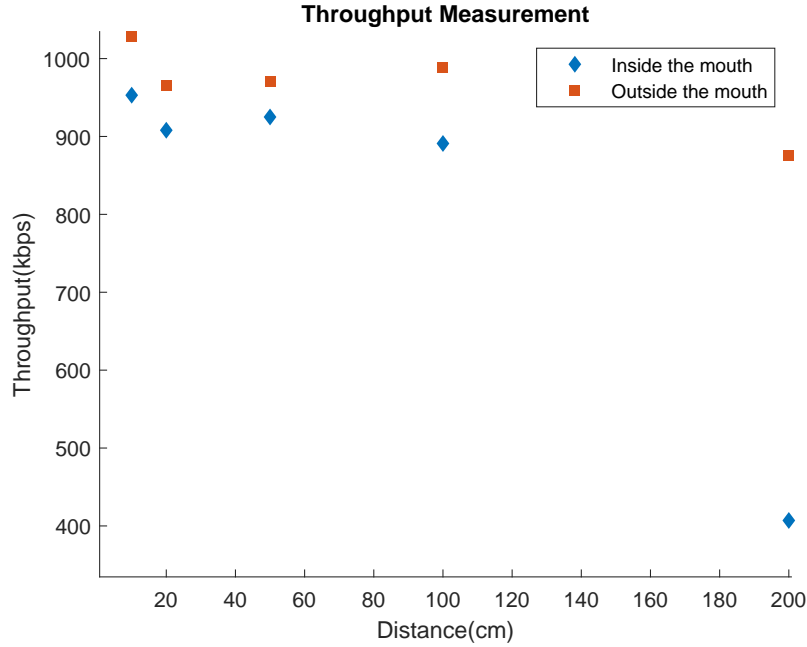


Figure 6.7: Throughput measurement

### 6.2.3 Power consumption

The power consumption of the complete evaluation prototype was measured through a battery depletion time test. The transmitter is configured to continuously transmit the simulated sensor data under the test cases illustrated in table. The advantages of this approach is that it provides an estimation of the power consumption under realistic usage scenarios. However several uncertainties arise due to the difficulties of estimating the exact state of the used battery. The tested battery is a 0.13 Wh battery measuring 12\*7\*5 mm and with a nominal voltage of 3.49 V. The provided battery life times provide a lower bound value.

Table 6.2: Peak current consumption - High Voltage mode

Test case	Link layer	Connection Interval [ms]	Update Rate [Hz]	Peak Current [mA]	Battery Life [Hours]
Maximal performance	2M	7.5	1120	9.3	3.14
Maximal range	Coded Phy	7.5	26	7.2	3.89
Balanced 1	2M	50	26	6.6	4.48
Maximal battery life	2M	400	26	6.6	4.48
Balanced 2	2M	7.5	100	6.9	3.93
Balanced 3	2M	7.5	400	7.0	3.93

The major parameter affecting the battery life is the connection interval of the Bluetooth transmitter. This parameter describes the time between two connection events. The

radio turns on every connection event and can send more than one packet. In the remaining time the transmitter sleeps and saves power. Choosing a lower connection interval results in a more robust connection however at the cost of a higher power consumption. When choosing a higher connection interval, the following situation might occur. If the first packet in a connection interval is dropped, the connection is dropped for the complete interval resulting in several lost packets. If the last packet in a connection interval is dropped this wouldn't have such a dire consequence. It was observed that lowering the transmission rate beyond a certain limit provided no additional power saving. However a lower transmission rate provides the transmitter to have more time to resend failed packets.

Additionally the rate at which the SoC updates the simulation values affects the power consumption. Here again we identify the compromise between connection performance and battery life. These parameters can be adaptively optimized depending on the usage scenario.

# **7** Chapter 7

## **Discussion**

---

The interaction of biological matter with a wireless link originating from inside the mouth results in the attenuation of the received signal at the receiver due to absorption and reflection at the interfaces. The absorption results from the conduction and displacement currents resulting from the propagation of an electromagnetic wave in a lossy medium. Additionally mouth cavity tissues are a layered structure composed of muscle, fat and skin and the oral mucosa. Each layer possess a different complex permittivity resulting in reflection and refraction at the interfaces.

An antenna placed close to biological tissue is detuned resulting in lower radiated power. This can be addressed by tuning the antenna by changing its physical dimensions or through an optimized radome.

An evaluation prototype was constructed using off the shelf components to quantify these losses. The complete prototype can be placed behind the lips and be completely discrete.

As expected when inserting the antenna inside the mouth the received signal strength is reduced. However by adjusting the connection parameters and transmission behavior a robust wireless link could still be achieved.

The criterion for the quality of the wireless link is the percentage of successfully validated simulation packets. The transmitter continuously sends a data sequence at an adjustable rate. The receiver validates the received data to obtain the good packet rate. Several connection parameters can be modified to optimize for power consumption, data rate or range. These parameters can be adjusted automatically depending on the usage scenario. We can identify two possible use cases. In the first use case the gesture recognition is done locally on the embedded SoC and data is only sent once a gesture is detected. Lower transmission rate is required in this case allowing the transmitter to sleep most of the time and save power. This can improve the power consumption from to as seen in.

In the second use case the user controls the mouse pointer on the screen. In this use case higher transmission rates are required. Setting the transmission rate too high results in an increase in dropped packets as the transmitter does not have enough time to retransmit the lost packets. Dropped packets are easily perceived when moving the mouse cursor and should be avoided.

Several advantages result from the usage of BLE5 as a communication protocol, such as the higher speed link layer 2M and the long range physical layer code phy. In addition BLE5 is backward compatible with BLE4 typically found in most smartphones and laptops. The major drawback of this communication protocol is the high latency of the communication.

The power consumption of the evaluation prototype was measured in a battery depletion test. Using a tiny 0.13 Wh battery, a battery life of 3.14 hours was obtained for the fastest transmission rate at 1KHz. At a more moderate 400 Hz transmission rate 4 hours was obtained. The maximal battery life was obtained at 4.48 when a higher connection interval was selected.

## 7.1 Potential improvements

- The used antenna is not optimized for intra-oral operation. A custom antenna with a reflection coefficient tuned to be in the frequency range of interest can provide an extended range and lower power consumption by reducing the transmit power.
- The Bluetooth protocol is complicated, has a lot of overhead and is not free for commercial usage. Implementing a custom protocol may result in a lower latency and better efficiency. The used SiP provides an API for the radio peripheral, making such an implementation easier. Custom communication protocols such as ESB or Gazelle are also supported and provided in the development kit.
- The used transmitter supports using a custom communication protocol alongside with Bluetooth Low Energy. This can be used when the user initiates mouse control movement to temporarily achieve faster transmission rates with lower latency without a need for reconnection.
- Wireless power harvesting techniques have been proven to penetrate body tissues. Such an implementation will result in a battery-less thinner intra-oral device. However the lower efficiency results in bigger batteries outside the mouth cavity and a receiver touching the face.

## 7.2 Overview and potential application

The provided implementation can be deemed adequate for an assistive device operating inside the mouth. In addition to the assistive context , we can identify several usage scenarios in which such a link can be used. Several biological metrics can be obtained from inside the mouth cavity such the pH level of saliva. These metrics can be collected and analyzed and have healthcare applications.

We can also identify several situations in which the hands can not be freely used. One such scenario is when playing the piano, in such context the user can use tongue movement to control the music recording environment or even play additional instruments using the tongue.

It was noted that perturbing the antenna with the tongue results in a measurable difference in the received RSSI value. This can be further investigated to develop passive sensors for detecting tongue movement.

# Bibliography

- [1] BELL, A. G.: On the production and reproduction of sound by light. In: *American Journal of Science* s3-20 (1880), oct, Nr. 118, S. 305–324. <http://dx.doi.org/10.2475/ajs.s3-20.118.305>. – DOI 10.2475/ajs.s3-20.118.305
- [2] CICHON, D.J.: The Heinrich Hertz wireless experiments at Karlsruhe in the view of modern communication. In: *International Conference on 100 Years of Radio*, IEE, 1995
- [3] RAYMER, Michael G.: *The Silicon Web*. CRC Press, 2009. <http://dx.doi.org/10.1201/9781439803127>. <http://dx.doi.org/10.1201/9781439803127>
- [4] SHI, Yao ; CHEN, Xing ; KIM, Hun-Seok ; BLAAUW, David ; WENTZLOFF, David: 28.3 A 606W mm-Scale Bluetooth Low-Energy Transmitter Using Co-Designed 3.5×3.5mm<sup>2</sup> Loop Antenna and Transformer-Boost Power Oscillator. In: *2019 IEEE International Solid-State Circuits Conference - (ISSCC)*, IEEE, feb 2019
- [5] BRANDL, M. ; GRABNER, J. ; KELLNER, K. ; SEIFERT, F. ; NICOLICS, J. ; GRABNER, S. ; GRABNER, G.: A Low-Cost Wireless Sensor System and Its Application in Dental Retainers. In: *IEEE Sensors Journal* 9 (2009), Nr. 3, S. 255–262
- [6] RAKIBET, Osman ; KELLY, Stephen ; HORNE, Robert ; BATCHELOR, John: Passive wireless tags for tongue controlled assistive technology interfaces. In: *Healthcare Technology Letters* 3 (2016), 02. <http://dx.doi.org/10.1049/htl.2015.0042>. – DOI 10.1049/htl.2015.0042
- [7] TAYLOR, P. S. ; BATCHELOR, J. C.: Small Epidermal UHF RFID Loop Antenna for Passive Oral Cavity Control Applications and Patient Health Monitoring. In: *2018 IEEE International Symposium on Antennas and Propagation USNC/URSI National Radio Science Meeting*, 2018, S. 687–688
- [8] WANG, Jingxian ; PAN, Chengfeng ; JIN, Haojian ; SINGH, Vaibhav ; JAIN, Yash ; HONG, Jason I. ; MAJIDI, Carmel ; KUMAR, Swarun: RFID Tattoo: A Wireless Platform for Speech Recognition. In: *Proc. ACM Interact. Mob. Wearable Ubiquitous Technol.* 3 (2019), Dezember, Nr. 4. <http://dx.doi.org/10.1145/3369812>. – DOI 10.1145/3369812

- [9] PENG, Qiyu ; BUDINGER, Thomas: ZigBee-based Wireless Intra-oral Control System for Quadriplegic Patients. In: *Conference proceedings : ... Annual International Conference of the IEEE Engineering in Medicine and Biology Society. IEEE Engineering in Medicine and Biology Society. Conference* 2007 (2007), 02, S. 1647–50. <http://dx.doi.org/10.1109/IEMBS.2007.4352623>. – DOI 10.1109/IEMBS.2007.4352623
- [10] JOHANSEN, Daniel ; CIPRIANI, Christian ; POPOVIC, Dejan ; STRUIJK, Lotte: Control of a Robotic Hand Using a Tongue Control System-A Prosthesis Application. In: *IEEE Transactions on Biomedical Engineering* 63 (2016), 01, S. 1–1. <http://dx.doi.org/10.1109/TBME.2016.2517742>. – DOI 10.1109/TBME.2016.2517742
- [11] STRUIJK, Lotte ; EGSGAARD, Line ; LONTIS, Eugen ; GAIHEDE, Michael ; BENTSEN, Bo: Wireless intraoral tongue control of an assistive robotic arm for individuals with tetraplegia. In: *Journal of NeuroEngineering and Rehabilitation* 14 (2017), 12. <http://dx.doi.org/10.1186/s12984-017-0330-2>. – DOI 10.1186/s12984-017-0330-2
- [12] STRUIJK, L. N. S. A. ; LONTIS, E. R. ; BENTSEN, B. ; CHRISTENSEN, H. V. ; CALTENCO, H. A. ; LUND, M. E.: Fully integrated wireless inductive tongue computer interface for disabled people. In: *2009 Annual International Conference of the IEEE Engineering in Medicine and Biology Society*, 2009, S. 547–550
- [13] LEE, Yongkuk ; HOWE, Connor ; MISHRA, Saswat ; LEE, Dong S. ; MAHMOOD, Musa ; PIPER, Matthew ; KIM, Youngbin ; TIEU, Katie ; BYUN, Hun-Soo ; COFFEY, James P. ; SHAYAN, Mahdis ; CHUN, Youngjae ; COSTANZO, Richard M. ; YEO, Woon-Hong: Wireless, intraoral hybrid electronics for real-time quantification of sodium intake toward hypertension management. In: *Proceedings of the National Academy of Sciences* 115 (2018), Nr. 21, 5377–5382. <http://dx.doi.org/10.1073/pnas.1719573115>. – DOI 10.1073/pnas.1719573115. – ISSN 0027-8424
- [14] PARK, H. ; GHovanloo, M.: Wireless Communication of Intraoral Devices and Its Optimal Frequency Selection. In: *IEEE Transactions on Microwave Theory and Techniques* 62 (2014), Nr. 12, S. 3205–3215
- [15] KONG, Fanpeng ; QI, Cheng ; LEE, Hoseon ; DURGIN, Gregory ; GHovanloo, Maysam: Antennas for Intraoral Tongue Drive System at 2.4 GHz: Design, Characterization, and Comparison. In: *IEEE Transactions on Microwave Theory and Techniques* PP (2018), 01, S. 1–10. <http://dx.doi.org/10.1109/TMTT.2017.2787118>. – DOI 10.1109/TMTT.2017.2787118
- [16] KONG, Fanpeng ; GHovanloo, Maysam ; DURGIN, Gregory D.: An Adaptive Impedance Matching Transmitter for a Wireless Intraoral Tongue-Controlled Assistive Technology. In: *IEEE Transactions on Circuits and Systems II: Express Briefs*

67 (2020), feb, Nr. 2, S. 240–244. <http://dx.doi.org/10.1109/tcsii.2019.2913623>. – DOI 10.1109/tcsii.2019.2913623

- [17] ORFANIDIS, Sophocles J.: *Electromagnetic Waves and Antennas*. Web page: [www.ece.rutgers.edu/orfanidi/ewa](http://www.ece.rutgers.edu/orfanidi/ewa) : Rutgers University, 2016
- [18] HUANG, Yi ; BOYLE, Kevin: *ANTENNAS FROM THEORY TO PRACTICE*. John Wiley Sons Ltd, 2008. – ISBN 978–0–470–51028–5
- [19] LI, C. ; SCHREURS, D.M.M.-P. ; HORNG, Changzhi Li Mohammad-Reza Tofighi Dominique Schreurs Tzyy-Sheng J. (Hrsg.): *Principles and Applications of RF/Microwave in Healthcare and Biosensing*. Joe Hayton, 2017. – 2–13 S. – ISBN 978–0–12–802903–9
- [20] In: MIKLAVĀIĀ, Damijan ; PAVĀJELJ, NataĀja ; HART, Francis X.: *Electric Properties of Tissues*. American Cancer Society, 2006. – ISBN 9780471740360
- [21] NIKOLOPOULOS, Chris D. ; BAKLEZOS, Anargyros T. ; CAPSALIS, Christos N.: AUTO RECONFIGURABLE PATCH ANTENNA FOR BIOMEDICAL SINGLE CHANNEL MULTI-FREQUENCY MICROWAVE RADIOMETRY APPLICATIONS. In: *Progress In Electromagnetics Research C* 49 (2014), S. 19–29. <http://dx.doi.org/10.2528/pierc14021904>. – DOI 10.2528/pierc14021904
- [22] REILLY, J. P.: *Applied Bioelectricity*. Springer New York, 1998. <http://dx.doi.org/10.1007/978-1-4612-1664-3>. <http://dx.doi.org/10.1007/978-1-4612-1664-3>
- [23] CAMPBELL, A.: Measurements and analysis of the microwave dielectric properties of tissues, 1990
- [24] MARGARET J. FEHRENBACH, Susan W. H.: *ILLUSTRATED ANATOMY OF THE HEAD AND NECK, FOURTH EDITION*. Saunders, 2011. – ISBN 978–1–4377–2419–6
- [25] BIJU-KUMAR, S. ; MATHEW, K.T. ; RAVEENDRANATH, U. ; AUGUSTINE, P.: Dielectric Properties of Certain Biological Materials at Microwave Frequencies. In: *Journal of Microwave Power and Electromagnetic Energy* 36 (2001), jan, Nr. 2, S. 67–75. <http://dx.doi.org/10.1080/08327823.2001.11688450>. – DOI 10.1080/08327823.2001.11688450
- [26] M, Pozar D.: *Microwave Engineering*. 4th. John Wiley Sons, Inc, 2012. – ISBN 978–0–470–63155–3
- [27] ZHOU, Gang ; HE, Tian ; KRISHNAMURTHY, Sudha ; STANKOVIC, John A.: Impact of radio irregularity on wireless sensor networks. In: *Proceedings of the 2nd international conference on Mobile systems, applications, and services - MobiSYS '04*, ACM Press, 2004

- [28] BACCIOR, Nouha ; KOUBÂA, Anis ; MOTTOLA, Luca ; ZÚÑIGA, Marco A. ; YOUSSEF, Habib ; BOANO, Carlo A. ; ALVES, Mário: Radio link quality estimation in wireless sensor networks. In: *ACM Transactions on Sensor Networks* 8 (2012), sep, Nr. 4, S. 1–33. <http://dx.doi.org/10.1145/2240116.2240123>. – DOI 10.1145/2240116.2240123
- [29] *nRF52840 Product Specification* [https://infocenter.nordicsemi.com/pdf/nRF52840\\_PS\\_v1.1.pdf](https://infocenter.nordicsemi.com/pdf/nRF52840_PS_v1.1.pdf).